## LETTER

## Prefrontal neuronal assemblies temporally control fear behaviour

 $\label{eq:cyril-Dejean} \ Cyril \ Dejean^{1,2*}, \ Julien \ Courtin^{1,2,3*}, \ Nikolaos \ Karalis^{1,2,4*}, \ Fabrice \ Chaudun^{1,2}, \ H\'el\`ene \ Wurtz^{1,2}, \ Thomas \ C. \ M. \ Bienvenu^{1,2} \ \& \ Cyril \ Herry^{1,2}$ 

Precise spike timing through the coordination and synchronization of neuronal assemblies is an efficient and flexible coding mechanism for sensory and cognitive processing 1-6. In cortical and subcortical areas, the formation of cell assemblies critically depends on neuronal oscillations, which can precisely control the timing of spiking activity<sup>7,8</sup>. Whereas this form of coding has been described for sensory processing and spatial learning<sup>9-12</sup>, its role in encoding emotional behaviour remains unknown. Fear behaviour relies on the activation of distributed structures, among which the dorsal medial prefrontal cortex (dmPFC) is known to be critical for fear memory expression<sup>13–16</sup>. In the dmPFC, the phasic activation of neurons to threat-predicting cues, a spike-rate coding mechanism, correlates with conditioned fear responses and supports the discrimination between aversive and neutral stimuli 14,17-19. However, this mechanism does not account for freezing observed outside stimuli presentations, and the contribution of a general spike-time coding mechanism for freezing in the dmPFC remains to be established. Here we use a combination of single-unit and local field potential recordings along with optogenetic manipulations to show that, in the dmPFC, expression of conditioned fear is causally related to the organization of neurons into functional assemblies. During fear behaviour, the development of 4 Hz oscillations coincides with the activation of assemblies nested in the ascending phase of the oscillation. The selective optogenetic inhibition of dmPFC neurons during the ascending or descending phases of this oscillation blocks and promotes conditioned fear responses, respectively. These results identify a novel phase-specific coding mechanism, which dynamically regulates the development of dmPFC assemblies to control the precise timing of fear responses.

To evaluate the contribution of prefrontal spike-time coding mechanisms to fear behaviour, mice were implanted with recording electrodes targeting the dmPFC and submitted to discriminative fear conditioning (Fig. 1a). In this behavioural model, mice learned to discriminate between two auditory stimuli of different frequency. The conditioned stimulus termed CS<sup>+</sup> is associated with the delivery of a mild foot-shock (the unconditioned stimulus, US) whereas a control stimulus, termed CS<sup>-</sup>, is not. Twenty-four hours after conditioning, when re-exposed to the CS<sup>+</sup> but not the CS<sup>-</sup>, mice displayed a selective increase in conditioned freezing, a characteristic fear immobilization reaction (Fig. 1a). Freezing was not only driven by CS sensory stimulations but was also observed between CS presentations, suggesting the involvement of internally generated mechanisms triggering/ maintaining freezing responses (Extended Data Fig. 1). Interestingly, during freezing, a subset of putative principal neurons (PNs) synchronized briefly and repeatedly, which represents a main characteristic of neuronal assemblies. To identify whether the formation of dmPFC assemblies may encode freezing, we investigated the presence of freezing-specific coactivation patterns in simultaneously recorded

dmPFC PNs (Extended Data Fig. 2). We calculated correlation matrices between spike trains of dmPFC PNs within a sliding window of 150 ms and performed principal component analyses on these correlation matrices (see Methods and Extended Data Fig. 3). In each animal, these analyses identified a discrete pattern of correlation that was freezing specific. This pattern corresponded to a subpopulation of PNs repeatedly recruited during freezing (Fig. 1b-d and Extended Data Fig. 3g). These dmPFC PNs displayed enhanced firing and coactivation each time the correlation pattern occurred, hence forming assemblies of PNs. These assembly neurons (ANs) were functionally segregated from ONs as coactivation between those two populations was not different from chance (Fig. 1d-f and Extended Data Fig. 3). Importantly, AN firing rate was stable during freezing, indicating that assembly detection was not due to tonic increase in firing (Fig. 1c and Extended Data Fig. 4a). During CS<sup>+</sup> presentations, the firing profile of dmPFC neurons was highly heterogeneous, with AN and ON exhibiting undifferentiated CS-evoked excitation, inhibition or no responses, as recently observed<sup>14,17</sup> (Extended Data Fig. 4c-f). In addition, the probability of observing assembly activation during freezing was similar inside or outside CS<sup>+</sup> presentations and did not vary around CS<sup>+</sup> presentations (Extended Data Fig. 4b, g). Together, these data indicate that a specific subpopulation of dmPFC PNs participates in functional assemblies during fear expression.

After conditioning, analyses of dmPFC local field potentials (LFPs) revealed a prominent oscillation in the 3-6 Hz range, with a peak around 4 Hz, which develops during freezing and temporally matched the recruitment of dmPFC assemblies (Fig. 2a-b). Consistent with our previous observations<sup>20</sup>, power spectral and spectrogram analyses indicated that dmPFC 4Hz oscillation power was significantly higher during freezing compared with mobility periods, and that freezing onset and offset coincided with an increase and decrease of 4 Hz power, respectively (Fig. 2c-d). Strikingly, frequency-specific correlational analyses revealed a significant and maximum correlation between dmPFC LFP 4Hz power and assembly probability within epochs surrounding freezing onset and offset (Fig. 2e). To evaluate whether the development of 4 Hz oscillations and the formation of dmPFC assemblies was predictive of freezing, we computed the first time point around freezing onset and offset for which 4 Hz oscillations and assembly probability significantly changed. These analyses indicated that both 4 Hz power and assembly activation significantly increased and decreased before freezing onset and offset, respectively (Fig. 2f). Importantly, the increase in 4 Hz power preceded the changes in assembly activation, which indicates that 4 Hz oscillations are a prerequisite process for dmPFC assembly activation and freezing onset. These data indicate that freezing dynamics are precisely controlled by a 4 Hz-mediated recruitment of dmPFC assemblies.

To understand how 4 Hz oscillations dynamically shape dmPFC assemblies during freezing, we evaluated the phase locking of

<sup>&</sup>lt;sup>1</sup>INSERM, Neurocentre Magendie, U862, 146 Rue Léo-Saignat, 33077 Bordeaux, France. <sup>2</sup>Université de Bordeaux, Neurocentre Magendie, U862, 146 Rue Léo-Saignat, 33077 Bordeaux, France. <sup>3</sup>Friedrich Miescher Institute for Biomedical Research, Maulbeerstrasse 66, CH-4058 Basel, Switzerland. <sup>4</sup>Faculty of Medicine, Ludwig-Maximilians Universität München, 82152 Planegg-Martinsried, Germany.

<sup>\*</sup>These authors contributed equally to this work.

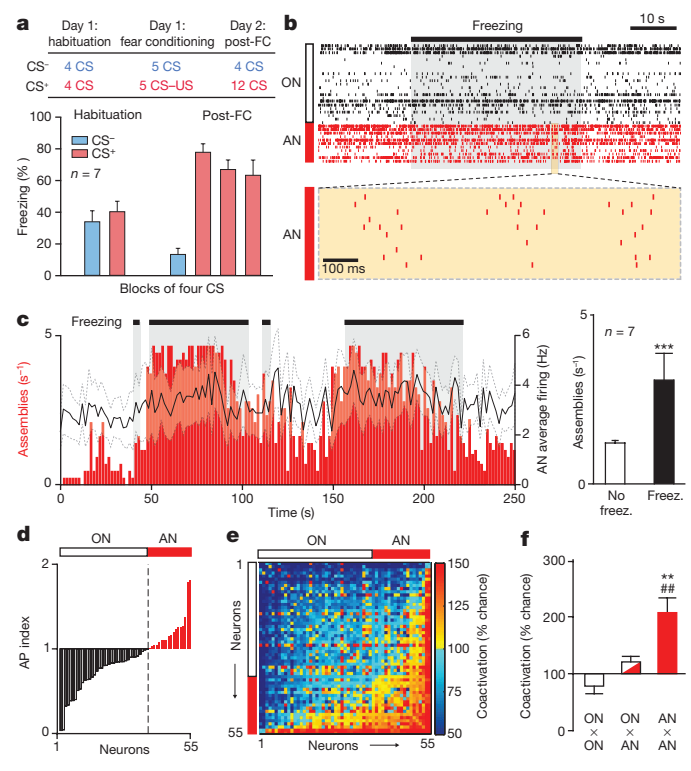


Figure 1 | dmPFC PNs participate in neuronal assemblies during freezing. a, Protocol and behavioural results. During habituation, mice (n=7) exhibited low freezing during CS<sup>-</sup> and CS<sup>+</sup>. After conditioning (post-FC), CS<sup>+</sup> induced high freezing compared with CS<sup>-</sup> (Friedman repeated-measures one-way analysis of variance (ANOVA) on ranks test, P < 0.01; Student-Newman-Keuls post-hoc test, CS<sup>-</sup> versus each CS<sup>+</sup> block, all P < 0.05). **b**, Example of dmPFC ANs exhibiting temporal organization during freezing compared with no freezing and to ON. c, Left: representative example of assembly activation during freezing versus no freezing and averaged firing for AN (n = 16, black line; white shaded area, s.e.m.). Grey shaded area represents freezing periods. Right: average numbers of assemblies activated during no freezing (No freez.) and freezing (Freez.) (n = 7 mice, Wilcoxon signed-rank test, no-freezing versus freezing, \*\*\*P < 0.001). **d**, Distribution of the assembly participation index (AP index) for 55 dmPFC PNs recorded in a mouse. The individual neuron AP index shows which PNs are significantly active (AN), or inhibited/unchanged (ON) within freezing patterns detected by principal component analysis (1, chance level). e, Coactivation matrix averaged over freezing epochs from the same 55 dmPFC PNs. The strength of the coactivation between neuron pairs is expressed as the percentage of coactivation compared with chance. f, Averaged coactivation for AN and/or ON pairs (one sample t-test, coactivation versus 100% hypothetical mean, P < 0.01; one-way ANOVA, P < 0.001; Bonferroni post-hoc test, AN × AN versus any other group, \*\*P < 0.01). Shaded areas and error bars, mean  $\pm$  s.e.m.

individual AN and ON to 4 Hz oscillations (Fig. 3a, b). The fraction of dmPFC neurons significantly phase-locked to 4 Hz oscillations was larger for ANs than ONs (Fig. 3c). Remarkably, phase-locked ANs were highly selectivity of 4 Hz ascending phase, while the preferred phase distribution of ONs was homogenous (Fig. 3d, e). To control if ANs might only synchronize because of their 4 Hz phase locking or to 4 Hz power increase, we first evaluated the averaged pairwise co-firing activity between pairs of ANs or ONs as a function of 4 Hz phase. This co-firing activity was corrected for the temporal and phase relation between pairs of neurons using a shuffling and shift predictor approach (see Methods and Fig. 3f). The corrected co-firing activity of AN was significantly stronger in the ascending compared with the descending phase of 4 Hz oscillation, which rules out the possibility that AN synchronization is solely due to AN phase locking (Fig. 3f). Next, we computed the corrected co-firing of AN pairs as a function of 4 Hz

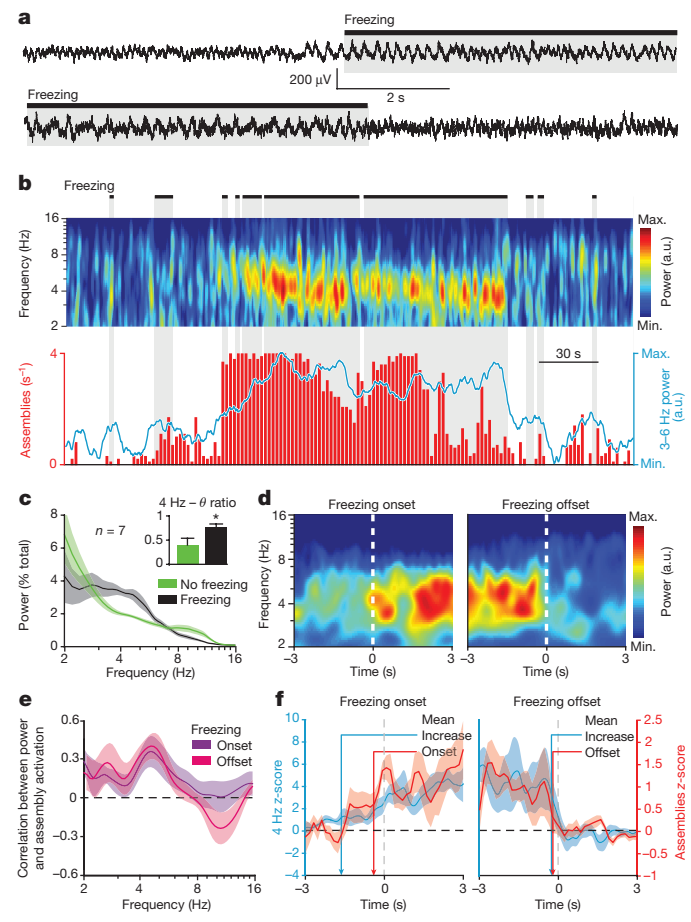


Figure 2 | Temporal matching of 4 Hz oscillations and dmPFC assemblies during freezing. a, Examples of raw dmPFC LFP traces at the onset (top) and offset (bottom) of a freezing episode. b, Freezing episodes (top, black lines and grey boxes), LFP spectrogram in the 2-16 Hz frequency band (middle, log<sub>2</sub> scale), assembly activation and LFP power averaged in the 3-6 Hz band (bottom). c, Normalized LFP power spectra for freezing and no freezing in the 2–16 Hz band (n = 7 mice;  $\log_2$  scale). Inset: 4 Hz to  $\theta$  ratio for freezing and no freezing (n = 7 mice, Wilcoxon signed-rank test, non-freezing versus freezing, \*P < 0.05). **d**, Averaged peri-event spectrogram in the 2-16 Hz frequency band (log<sub>2</sub> scale) centred on freezing onset (left, n = 7 mice) and offset (right, n = 7 mice). e, Correlation between power and assembly activation as a function of LFP frequency (log<sub>2</sub> scale) during epochs surrounding freezing onset (-3 s to +3 s, purple line, n=7 mice) and offset (-3 s to +3 s, pink line,n = 7 mice). The y axis represents the Spearman correlation coefficient. f, Normalized 3–6 Hz power and assembly activation z-score centred on freezing onset (left, n = 7 mice) and offset (right, n = 7 mice). Arrows indicate the first time point with a significant increase around freezing onset or decrease around freezing offset. Shaded areas and error bars, mean  $\pm$  s.e.m.; a.u., arbitrary units.

power levels and phases (Fig. 3g). We observed that, for different power levels, synchronization among AN, but not ON, was restricted to the ascending phase of the oscillations and larger than ON synchronization (Fig. 3g). These data indicate that the coordination of dmPFC PNs into cell assemblies during freezing is orchestrated by 4 Hz oscillations.

To evaluate whether the formation of dmPFC assemblies was causally related to freezing expression, we used an optogenetic strategy based on the selective activation of dmPFC parvalbumin-expressing interneurons (PV<sup>+</sup>) in the ascending or descending phase of 4 Hz oscillations (see Methods, Fig. 4 and Extended Data Fig. 5a, b). Conditional adeno-associated virus (AAV) encoding for channelrhodopsin (ChR2) was injected in the dmPFC of mice expressing the Cre recombinase under the control of a PV promoter to specifically infect PV<sup>+</sup> interneurons (Fig. 4 and Extended Data Fig. 5a, b). Because

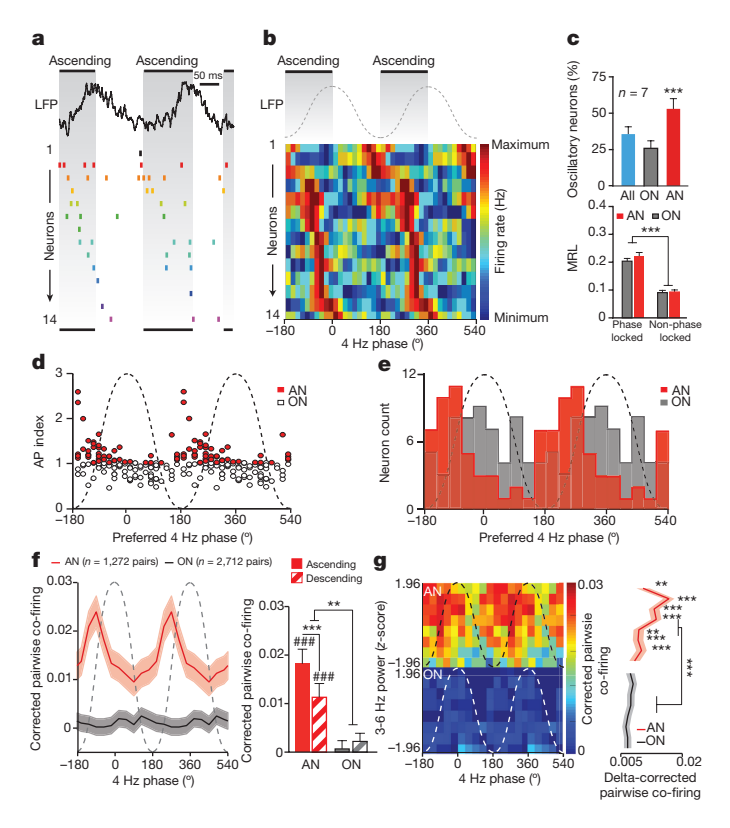
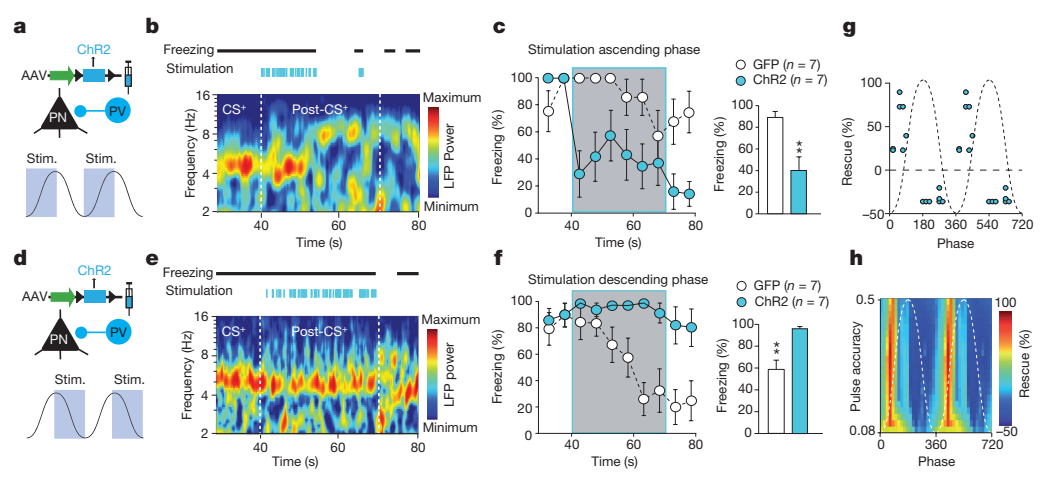


Figure 3 | Four-hertz oscillations organize dmPFC PNs into assemblies during freezing. a, Representative example of an LFP recorded in the dmPFC showing prominent 4 Hz oscillations and simultaneous sequential activation of 14 AN recorded in the same animal during freezing. b, Averaged firing of individual AN displayed in a as a function of 4 Hz LFP oscillation phase. Each AN was significantly modulated by 4 Hz phase (Rayleigh test, all P < 0.05). c, Top: average percentage of neurons significantly phase-locked to 4 Hz oscillations among all neurons (blue), AN (red) and ON (white) (n = 7 mice, one way repeated-measures ANOVA, P < 0.001; Bonferroni post-hoc test, \*\*\*P < 0.001). Bottom: averaged mean resultant length vector (MRL) for phase-locked and nonphase-locked AN and ON neurons (n = 7 mice, AN: n = 50/90 phaselocked neurons; ON: n = 61/200 phase-locked neurons; two-way ANOVA,  $F_1$ : AN versus ON, P = 0.206;  $F_2$ : phase-locking, P < 0.001;  $F_1 \times F_2$ : P = 0.324; Bonferroni post-hoc test, \*\*\*P < 0.001). **d**, Distribution of all phase-locked dmPFC PNs assembly participation indices (AP index) as a function of preferred phase (left axis, red dots: AN, AP index > 1, n = 50neurons; white dots: ON, AP index < 1, n = 61 neurons; bin: 18°, n = 7mice). e, Distribution of phase-locked AN and ON preferred phases (AN: n = 50 neurons; ON: n = 61 neurons; bin: 18°, n = 7 mice). f, Left: corrected pairwise co-firing activity of pairs of AN and ON as a function of 4 Hz phase (AN = 1,272 pairs; ON = 2,712 pairs recorded in 7 mice). Right: averaged corrected pairwise co-firing for AN and ON neurons during the ascending or descending phase of 4 Hz oscillations (n = 7 mice, AN: n = 1,272 pairs, ON: n = 2,712 pairs, two-way ANOVA,  $F_1$ : AN versus ON, P = 0.003;  $F_2$ : ascending versus descending, P < 0.001;  $F_1 \times F_2$ : P < 0.001; Bonferroni post-hoc test, \*\*P < 0.01, \*\*\*P < 0.001; one sample t-test against hypothetical mean = 0, P < 0.001). h, Left: corrected pairwise co-firing activity as a function of the phase and power (*z*-score) of 4 Hz oscillations. Right: delta-corrected pairwise co-firing activity (maximum ascending minus minimum descending phase) of pairs of AN and ON (AN = 1,272 pairs; ON = 2,712 pairs recorded in 7 mice; two-way ANOVA, $F_1$ : AN versus ON, P < 0.001;  $F_2$ : power, P < 0.001;  $F_1 \times F_2$ : P < 0.001; Bonferroni post-hoc AN versus ON, \*\*P < 0.01, \*\*\*P < 0.001; one sample *t*-test against hypothetical mean = 0, P < 0.001). Error bars, mean  $\pm$  s.e.m.

dmPFC assemblies are both phase- and freezing-specific, we recorded and performed online detection of freezing, high instantaneous power and ascending phase of 4 Hz oscillations in the period after a train of CS<sup>+</sup> presentations (See methods, Extended Data Fig. 6). Each time these conditions were fulfilled, we optogenetically activated dmPFC PV<sup>+</sup>

interneurons to inhibit PN firing at the ascending or descending phase of 4 Hz oscillations (Fig. 4a, d and Extended Data Figs 5–7). During post-CS<sup>+</sup> presentations, green fluorescent protein (GFP) controls exhibited high fear levels on day 2 and low fear levels on days 3 and 4, which represent a natural timing effect, not a bias of our experimental conditions (Extended Data Fig. 6c). Importantly, activating or inhibiting PV<sup>+</sup> interneurons in the ascending or descending phase of 4Hz oscillations did not modify 4 Hz power compared with periods without stimulation or GFP controls (Extended Data Fig. 5d-i). In contrast, the activation or inhibition of PV<sup>+</sup> interneurons in the ascending or descending phase of 4 Hz oscillations respectively reduced and increased the co-firing activity of dmPFC PNs in the phase targeted (Extended Data Fig. 8c, d). Optogenetic-mediated inhibition of dmPFC PNs in the ascending phase of the oscillation significantly reduced freezing compared with control conditions (Fig. 4b, c, g, h and Extended Data Fig. 6). To evaluate the temporal specificity of our manipulation, we inhibited the firing of dmPFC PNs in the descending phase of the oscillation during freezing, when dmPFC ANs are less likely to be coactive (Fig. 3d-f). This manipulation significantly increased freezing compared with control conditions (Fig. 4e-h and Extended Data Fig. 6). Importantly, because we performed these optogenetic manipulations over 2 days (Extended Data Fig. 6d), we ensured that the stimulation in the ascending phase of 4 Hz oscillations on the first day had no influence on CS<sup>+</sup>-evoked freezing the next day (Extended Data Fig. 6g). Finally, we repeated our stimulation experiment in mice in which PV<sup>+</sup> interneurons expressed archeorhodopsin (ArchT) to inhibit dmPFC PV<sup>+</sup> interneurons and thereby disinhibit dmPFC PNs (Extended Data Fig. 9). When applied in the descending phase of the oscillation, stimulation had no effect on freezing (Extended Data Fig. 9b, c). However, in the ascending phase of the oscillation, PN disinhibition produced a significant increase in freezing (Extended Data Fig. 9d, e). Together, these results demonstrate that the formation of dmPFC assemblies at the ascending phase of 4 Hz oscillations and their suppression in the descending phase are necessary for the precise temporal coding of fear behaviour.

Using single-unit and LFP recordings and optogenetic manipulations, we demonstrated that a subset of dmPFC PNs participate in the formation of functional assemblies, dynamically coordinated by 4 Hz oscillations during freezing. Our results indicate that the formation of dmPFC assemblies at specific phases of 4 Hz oscillations is causally related to freezing expression. Importantly, although the strength of phase locking or the increase in 4 Hz power might impact neuronal synchronization among ANs, our analyses indicate that they cannot explain alone the specific and stronger synchronization we observed between AN (Fig. 3f, g). Therefore the temporal organization of ANs in the ascending phase of 4 Hz oscillations appears as a specific encoding mechanism for freezing. Modification of dmPFC spiking activity after presentations of threat-predicting cues, a form of rate coding mechanism that correlates with fear responses, has been described in the past<sup>14,17,18,21</sup> and could be related to plasticity mechanisms or attentional processes. Our data indicate that, in addition to this mechanism, the expression of conditioned freezing is also encoded in the dynamic organization of internally generated dmPFC assemblies. To our knowledge, these data represent the first causal demonstration of a phase-specific coding mechanism during conditioned fear behaviour. In a recent study, we imposed a 4 Hz analogue stimulation to the dmPFC through PV<sup>+</sup> interneurons and showed that this artificial rhythm was sufficient to elicit freezing and fear memory<sup>20</sup>. The concept in the present model is radically different in that we did not impose the rhythm but intended to interfere with dmPFC assemblies nested in the ascending phase of 4 Hz oscillations, which were specifically activated during fear expression (see Supplementary Information for further discussion). Whereas 4 Hz oscillations have already been described in different structures during various behavioural tasks<sup>20,22–25</sup>, the origin of this slow oscillation is still unknown. It was suggested that this oscillation originates from the ventral tegmental area<sup>24</sup>, or



**Figure 4** | **Phase-specific optogenetic inhibition of dmPFC PNs controls freezing. a, d,** Schematic of the strategy used to inhibit dmPFC PNs during the ascending or descending phase of 4 Hz oscillation. Stim., stimulation. **b, e,** Top: representative example of freezing (black line) and kinetics of light pulse stimulations (blue ticks) during and after CS<sup>+</sup> presentations 24 h (**b**) and 48 h (**e**) after conditioning. Bottom: corresponding LFP spectrogram in the 2–16 Hz band (binary logarithmic scale) during light-mediated inhibition of dmPFC assemblies in the ascending (**b**) or descending (**e**) phase of the oscillation. **c, f,** Left: time-resolved changes in freezing during light-mediated inhibition of dmPFC assemblies in the ascending (**c**) or descending (**f**) phase of the 4 Hz oscillation in PV-IRES-Cre mice infected within the dmPFC with ChR2 (ascending phase: first CS<sup>+</sup>, *n* = 7; descending phase: first CS<sup>+</sup>, *n* = 7; descending phase: first CS<sup>+</sup>, *n* = 7; descending phase: first CS<sup>+</sup>, *n* = 7; ascending phase:

two-way ANOVA, factor 1: ChR2 versus GFP, P < 0.001; factor 2: time, P < 0.001;  $F_1 \times F_2$ , P < 0.05; descending phase: two-way ANOVA, factor 1: ChR2 versus GFP, P < 0.001; factor 2: time, P < 0.001;  $F_1 \times F_2$ , P < 0.05). Shaded area represents light stimulation period. Right: averaged freezing from PV-IRES-Cre mice infected in dmPFC with ChR2 (n = 7) or GFP (n = 7) during the stimulation (Mann–Whitney test, ChR2 versus GFP, \*\*P < 0.01). **g**, **h**, Percentage of freezing rescue (freezing for ChR2 minus average freezing for GFP) as a function of the phase of the stimulation (**g**), or as a function of both the phase and pulse stimulation accuracy (**h**) for mice stimulated in the ascending or descending phase of the 4 Hz oscillation (n = 25 sessions in 16 animals). Pulse stimulation accuracy to the phase of 4 Hz oscillations was quantified using MRL of pulse locking on 4 Hz phase. Error bars, mean  $\pm$  s.e.m.

the whisker barrel cortex<sup>26</sup>. Our data demonstrate that the encoding of distinct behavioural states occurs through the dynamic organization of dmPFC assemblies by 4 Hz oscillations. However, it is still not clear how this phase-specific code is relayed to downstream structures to actively drive or suppress freezing. Recent data demonstrated that the synchronization of slow oscillations between dmPFC and amygdala circuits correlates with freezing<sup>19,27,28</sup>. This could represent an effective mechanism for the coincident activation of neurons within distributed brain regions. To model the relationship between dmPFC phase-coding and freezing expression, we propose a functional scheme where dmPFC assembly activation is at the core of an emitter-receiver system for fear expression (Extended Data Fig. 10a). In this system, dmPFC assembly activity emerges from background activity because of its phase specificity. This temporal constraint provides a clear signal-to-noise ratio within an entire 4 Hz cycle (SNR) for a receiver, which could be the amygdala as recently suggested 19,20,27,28. In this model, the effects of the optogenetic manipulations on freezing can be explained by alterations of the transmission of this dmPFC-to-receiver fear signal. On the one hand, upregulation of SNR through dmPFC PN inhibition during the descending phase (Extended Data Fig. 10b) or disinhibition during the ascending phase (Extended Data Fig. 10c) enhanced fear expression. On the other hand, downregulation of SNR through dmPFC PN ascending phase inhibition (Extended Data Fig. 10b) reduced freezing. Beyond the field of emotions, this mechanism is likely to apply to other brain functions that depend on the activation of assemblies through oscillatory processes<sup>1-6</sup>. Finally, as previously hypothesized<sup>29</sup>, our data confirm that the persistence of fear, which is a core symptom of anxiety disorders, could be precisely controlled by the modulation of activity in relation to specific slow oscillations.

**Online Content** Methods, along with any additional Extended Data display items and Source Data, are available in the online version of the paper; references unique to these sections appear only in the online paper.

Received 11 November 2015; accepted 8 June 2016. Published online 13 July 2016.

- Gire, D. H. et al. Temporal processing in the olfactory system: can we see a smell? Neuron 78, 416–432 (2013).
- Friedrich, R. W., Habermann, C. J. & Laurent, G. Multiplexing using synchrony in the zebrafish olfactory bulb. Nature Neurosci. 7, 862–871 (2004).
- Igarashi, K. M., Lu, L., Colgin, L. L., Moser, M. B. & Moser, E. I. Coordination of entorhinal-hippocampal ensemble activity during associative learning. *Nature* 510, 143–147 (2014).
- Pastalkova, E., Itskov, V., Amarasingham, A. & Buzsáki, G. Internally generated cell assembly sequences in the rat hippocampus. Science 321, 1322–1327 (2008).
- Huxter, J., Burgess, N. & O'Keefe, J. Independent rate and temporal coding in hippocampal pyramidal cells. Nature 425, 828–832 (2003).
- O'Neill, J., Senior, T. J., Allen, K., Huxter, J. R. & Csicsvari, J. Reactivation of experience-dependent cell assembly patterns in the hippocampus. *Nature Neurosci.* 11, 209–215 (2008).
- Harris, K. D., Csicsvari, J., Hirase, H., Dragoi, G. & Buzsáki, G. Organization of cell assemblies in the hippocampus. *Nature* 424, 552–556 (2003).
- Buzsáki, G. Neural syntax: cell assemblies, synapsembles, and readers. Neuron 68, 362–385 (2010).
- Dupret, D., O'Neill, J., Pleydell-Bouverie, B. & Csicsvari, J. The reorganization and reactivation of hippocampal maps predict spatial memory performance. *Nature Neurosci.* 13, 995–1002 (2010).
- Huxter, J. R., Senior, T. J., Allen, K. & Csicsvari, J. Theta phase-specific codes for two-dimensional position, trajectory and heading in the hippocampus. *Nature Neurosci.* 11, 587–594 (2008).
- Richmond, B. J., Optican, L. M., Podell, M. & Spitzer, H. Temporal encoding of two-dimensional patterns by single units in primate inferior temporal cortex. I. Response characteristics. J. Neurophysiol. 57, 132–146 (1987).
- Laurent, G., Wehr, M. & Davidowitz, H. Temporal representations of odors in an olfactory network. J. Neurosci. 16, 3837–3847 (1996).
- Corcoran, K. A. & Quirk, G. J. Activity in prelimbic cortex is necessary for the expression of learned, but not innate, fears. J. Neurosci. 27, 840–844 (2007).
- Courtin, J. et al. Prefrontal parvalbumin interneurons shape neuronal activity to drive fear expression. Nature 505, 92–96 (2014).
- Vidal-Gonzalez, I., Vidal-Gonzalez, B., Rauch, S. L. & Quirk, G. J. Microstimulation reveals opposing influences of prelimbic and infralimbic cortex on the expression of conditioned fear. *Learn. Mem.* 13, 728–733 (2006).
- Do-Monte, F. H., Quiñones-Laracuente, K. & Quirk, G. J. A temporal shift in the circuits mediating retrieval of fear memory. *Nature* 519, 460–463 (2015).
- Burgos-Robles, A., Vidal-Gonzalez, I. & Quirk, G. J. Sustained conditioned responses in prelimbic prefrontal neurons are correlated with fear expression and extinction failure. J. Neurosci. 29, 8474–8482 (2009).
- Chang, C. H., Berke, J. D. & Maren, S. Single-unit activity in the medial prefrontal cortex during immediate and delayed extinction of fear in rats. PLoS ONE 5, e11971 (2010).

## RESEARCH LETTER

- Likhtik, E., Stujenske, J. M., Topiwala, M. A., Harris, A. Z. & Gordon, J. A. Prefrontal entrainment of amygdala activity signals safety in learned fear and innate anxiety. *Nature Neurosci.* 17, 106–113 (2014).
- Karalis, N. et al. 4-Hz oscillations synchronize prefrontal–amygdala circuits during fear behavior. Nature Neurosci. 19, 605–612 (2016).
- Livneh, U. & Paz, R. Amygdala-prefrontal synchronization underlies resistance to extinction of aversive memories. *Neuron* 75. 133–142 (2012).
- Dzirasa, K. et al. Lithium ameliorates nucleus accumbens phase-signaling dysfunction in a genetic mouse model of mania. J. Neurosci. 30, 16314–16323 (2010).
- Dzirasa, K., Fuentes, R., Kumar, S., Potes, J. M. & Nicolelis, M. A. Chronic in vivo multi-circuit neurophysiological recordings in mice. J. Neurosci. Methods 195, 36–46 (2011).
- Fujisawa, S. & Buzsáki, G. A 4 Hz oscillation adaptively synchronizes prefrontal, VTA, and hippocampal activities. *Neuron* 72, 153–165 (2011).
- Tort, A. B. et al. Dynamic cross-frequency couplings of local field potential oscillations in rat striatum and hippocampus during performance of a T-maze task. Proc. Natl Acad. Sci. USA 105, 20517–20522 (2008).
- Ito, J. et al. Whisker barrel cortex delta oscillations and gamma power in the awake mouse are linked to respiration. Nature Commun. 5, 3572 (2014).
- Lesting, J. et al. Patterns of coupled theta activity in amygdala-hippocampalprefrontal cortical circuits during fear extinction. PLoS ONE 6, e21714 (2011).
- Stujenske, J. M., Likhtik, E., Topiwala, M. A. & Gordon, J. A. Fear and safety engage competing patterns of theta-gamma coupling in the basolateral amygdala. *Neuron* 83, 919–933 (2014).

 Dejean, C. et al. Neuronal circuits for fear expression and recovery: recent advances and potential therapeutic strategies. *Biol. Psychiatry* 78, 298–306 (2015).

Supplementary Information is available in the online version of the paper.

Acknowledgements We thank the members of the Herry laboratory for comments on the manuscript, and K. Deisseroth and E. Boyden for sharing material. Microscopy was done in the Bordeaux Imaging Center of the CNRS-INSERM and Bordeaux University, a member of France Biolmaging. This work was supported by grants from the French National Research Agency (ANR-10-EQPX-08 OPTOPATH; LABEX BRAIN ANR 10-LABX-43, LABEX TRAIL ANR 10-LABX-57), the European Research Council (ERC) under the European Union's Seventh Framework Program (FP7/2007-2013)/ERC grant agreement number 281168, and the Conseil Regional d'Aquitaine.

**Author Contributions** F.C., J.C., C.D., N.K., T.C.M.B. and H.W. performed the experiments and analysed the data. J.C., C.D. and C.H. designed the experiments and wrote the paper.

**Author Information** Reprints and permissions information is available at www.nature.com/reprints. The authors declare no competing financial interests. Readers are welcome to comment on the online version of the paper. Correspondence and requests for materials should be addressed to C.D. (cyril.dejean@scilight.eu) or C.H. (cyril.nerry@inserm.fr).

**Reviewer Information** *Nature* thanks A. Holmes, P. O'Donnell and the other anonymous reviewer(s) for their contribution to the peer review of this work.

## **METHODS**

Animals. Male C57BL6/J mice (3 months old, Janvier), PV-IRES-Cre mice (3 months old, Jackson Laboratory, B6;129P2-Pvalbtm1(cre)Arbr/J) and CamKIIalpha-Cre mice (3 months old, Jackson Laboratory, B6.Cg-Tg(Camk2A-cre)T29-1Stl/J) were individually housed for at least 7 days before all experiments, under a 12-h light-dark cycle, and provided with food and water *ad libitum*. All procedures were performed in accordance with standard ethical guidelines (European Communities Directive 86/60-EEC) and were approved by the committee on Animal Health and Care of Institut National de la Santé et de la Recherche Médicale and French Ministry of Agriculture and Forestry (agreement A3312001). Representative examples and traces displayed in the main figures were observed for the seven animals used in these experiments.

Behaviour. Fear conditioning and testing took place in two different contexts (contexts A and B). The conditioning and testing boxes were cleaned with 70% ethanol and 1% acetic acid before and after each session, respectively. To score freezing behaviour, an automated infrared beam detection system located on the bottom of the experimental chambers was used (Coulbourn Instruments). Because the detection of our dependent variable (freezing) was independent of the experimenter, we did not use a blinding process for group allocation or behaviour scoring. The animals were considered to be freezing if no movement was detected for 2 s. On day 1, C57BL6/J mice were submitted to a habituation session in context A, in which they received four presentations of the CS<sup>+</sup> and the CS<sup>-</sup> (total CS duration 30 s, consisting of 50-ms pips at 0.9 Hz repeated 27 times, 2 ms rise and fall; pip frequency 7.5 kHz or white-noise, 80 dB sound pressure level). Discriminative fear conditioning was performed on the same day by pairing the CS<sup>+</sup> with a US (1-s foot-shock, 0.6 mA, 5 CS<sup>+</sup>-US pairings; inter-trial intervals, 20–180 s). The onset of the US coincided with the offset of the CS<sup>+</sup>. The CS<sup>-</sup> was presented after each CS<sup>+</sup>-US association but was never reinforced (five CS<sup>-</sup> presentations; intertrial intervals, 20-180 s). The frequencies used for CS<sup>+</sup> and CS<sup>-</sup> were counterbalanced across animals and randomization of CS<sup>-</sup> and CS<sup>+</sup> allocation was performed using an online randomization algorithm (http://www.randomization.com/). On day 2, conditioned mice were submitted to a post-fear-conditioning session in context B during which they received 4 and 12 presentations of the CS<sup>-</sup> and CS<sup>+</sup>, respectively. Seven naive C57BL6/J mice were included in this experiment and the data were collected in two distinct replicates. For optogenetic experiments using channelrhodopsin (ChR2), archeorhodopsin (ArchT) or GFP controls, PV-IRES-Cre mice were submitted to the same conditioning protocol described above except that on days 2, 3 and 4, conditioned mice were submitted to post-fear-conditioning sessions in context B during which they received four presentations of the CSfollowed by four presentations of the CS<sup>+</sup>. The number of CS<sup>+</sup> was limited to four to prevent fear memory extinction from day 2 to days 3 and 4. Blue (ChR2) or Yellow (ArchT) light stimulation was applied during 30 s after the last pip of the four CS<sup>+</sup>. The rationale behind this stems from our previous study<sup>12</sup> showing that manipulation of CS<sup>+</sup>-evoked dmPFC activity impacted fear expression. To avoid interference with this activity period, the present manipulations were restricted to those 30 s immediately after sound presentation. Importantly, freezing levels on day 1 were of similar magnitude in GFP control and wild-type animals used in the first part of this study (Extended Data Fig. 6a, b). Typically, freezing levels in GFP controls during CS<sup>+</sup> were not different from day 2 to days 3 and 4 (Extended Data Fig. 6c). However, freezing level observed in the 30 s time windows after CS<sup>+</sup> went from high on day 2 to moderate on days 3 and 4 (Extended Data Fig. 6c). Our hypothesis predicts that 4 Hz ascending phase inhibition of PNs will decrease freezing and conversely for a stimulation in the descending phase. To evaluate the changes in freezing levels upon optogenetic stimulation, this behavioural pattern brought us to test ascending phase stimulation on day 2 and descending phase on day 3 to avoid floor and ceiling effect respectively (Extended Data Fig. 6d). For the same reasons, 4 Hz descending and ascending phase disinhibition of PNs were performed on days 3 and 4, respectively (Extended Data Fig. 9a). We also noticed a tendency for optogenetic stimulation to decrease freezing level around subsequent CS<sup>+</sup> on the same day in the ChR2 group (Extended Data Fig. 6e, f). To rule out the possibility that changes in freezing behaviour upon optogenetic stimulation were not solely due to the direct action of the stimulation but also to a cumulative effect of past manipulations, our analyses were restricted to the 30 s epoch after the first CS+ on days 2, 3 and 4. Although this decrease was not observed with ArchT animals (Extended Data Fig. 9b, d) we used the same restriction with this group for the sake of consistency with ChR2 group. Note that within these 30 s, light application was conditioned to the behaviour and the brain state of the animal (see section on 'Closed-loop stimulation'). To score freezing behaviour, the aforementioned automated infrared beam detection was used in addition to a Cineplex video tracking system (Plexon) that was used for online detection of freezing and subsequent conditional optogenetic stimulation. For optogenetic experiments, four distinct behavioural experiments were performed to collect the entire data set. The impact of stimulation pulse phase specificity on freezing behaviour was assessed by calculating freezing rescue as a function of pulses preferred 4Hz phase as well as phase locking strength. Freezing rescue was calculated as the difference between the average freezing levels of GFP control and that of ChR2 animal during optical stimulation epochs. Stimulation pulses preferred phase was retrieved through the pulse phase histogram and tested for significance (Rayleigh's test P). Pulse accuracy was quantified by phase locking strength using the mean resultant length (MRL): that is, the length of the mean vector. Low or high MRL values are respectively indicative of a spread or a concentrated circular distribution of pulses around the preferred phase. In a first set of analyses we considered only those experiments with canonic features (Fig. 4a–g): that is, where pulse phase distribution was significant (P < 0.05), preferred phase was in the intended range (ascending phase, -180 to 0°; descending phase, 0-180°) and MRL was above 0.2. For ArchT experiments, five animals fulfilled the criteria on days 3 and 4. For ChR2 experiments, on day 2 (ascending phase) seven animals fulfilled the criteria; on day 3 (descending phase) seven animals fulfilled the criteria. In a second set of experiment (Fig. 4h) we addressed the joint impact of phase and pulse accuracy on freezing level. For that purpose, we added sessions with weak MRL values to the previous set of analysed data. On day 2 (ascending phase) 14 sessions fulfilled the criteria; on day 3 (descending phase) 11 sessions fulfilled the criteria. That is a total of 25 sessions that were acquired in 16 animals as follows: 9 animals on both days 2 and 3; 5 animals only on day 2; and 2 animals only on day 3. The distributions of pulse accuracy (MRL) and preferred phase were then two-dimensionally interpolated to create a linearly spaced grid of freezing rescue value (bin MRL 0.02; bin phase 36°).

Surgery and recordings. Mice were anaesthetized with isoflurane (induction 3%, maintenance 1.5%) in oxygen. Body temperature was maintained at 37 °C with a temperature controller system (FHC). Mice were secured in a stereotaxic frame and unilaterally implanted in the left dorsomedial prefrontal cortex (dmPFC) with a multi-wire electrode array aimed at the following coordinates: 2 mm anterior to bregma;  $0.3 \, \text{mm}$  lateral to the midline; and  $0.8 - 1.4 \, \text{mm}$  ventral to the cortical surface. The electrodes consisted of 16 or 32 individually insulated nichrome wires (13  $\mu$ m diameter, impedance 30–100 k $\Omega$ ; Kanthal) contained in a 26-gauge stainless-steel guide cannula. The wires were attached to an 18-pin connector (Omnetics) or 2 connectors in the case of a 32-wire assembly. All implants were secured using Super-Bond cement (Sun Medical). After surgery mice were allowed to recover for 7 days and were habituated to handling. Analgesia was applied before, and 1 day after surgery (Metacam, Boehringer). Electrodes were connected to one or two headstages (Plexon) containing 16 unity-gain operational amplifiers. Each headstage was connected to a 16-channel preamplifier (gain 100 × bandpass filter from 150 Hz to 9 kHz for unit activity and from 0.7 Hz to 170 Hz for field potentials, Plexon). Spiking activity was digitized at 40 kHz and bandpass filtered from 250 Hz to 8 kHz, and isolated by time-amplitude window discrimination and template matching using a Multichannel Acquisition Processor system (Plexon). At the conclusion of the experiment, recording sites were marked with electrolytic lesions before perfusion, and electrode tips locations were reconstructed with standard histological techniques.

Virus injections and optogenetics. For optical control of PV interneurons, conditional AAV encoding ChR2 (AAV-EF1a-DIO-hChR2(H134R)-EYFP, serotype 5, Vector Core, University of North Carolina) or ArchT (AAV-FLEX-ArchT-GFP, serotype 9, Vector Core, University of North Carolina) were bilaterally injected into the dmPFC of PV-IRES-Cre mice from glass pipettes (tip diameter 10–20 µm) connected to a picospritzer (Parker Hannifin Corporation; approximately  $0.4\mu L$  per hemisphere) at the following coordinates: 2 mm anterior to bregma; 0.4 mm lateral to midline and 0.9 to 1.2 mm ventral to the cortical surface. One to two weeks after the injection mice were implanted bilaterally with optic fibres (diameter: 200 µm; numerical aperture: 0.37; flat tip; Doric Lenses) at the same coordinates. Control experiments were performed using an AAV containing the DNA construct for only GFP (AAV-FLEX-GFP, Vector Core, University of North Carolina). All implants were secured using Super-Bond cement (Sun Medical). For experiments using optogenetic stimulation coupled to single-unit recordings, one of the two optic fibres was combined to the array of 16 or 32 individually insulated nichrome wires. Single-unit recordings during the manipulation of PV interneurons were performed as described in the 'Surgery and recordings' section. Behavioural and recording experiments were performed 3-5 weeks after injection. The light (approximately 14 mW per implanted fibre) was bilaterally conducted from the laser (OptoDuet 473/593 nm, Ikecool) to the mice via two fibre-optic patch cords (diameter 200 µm, Doric Lenses), connected to a rotary joint (1  $\times$  2 fibre-optic rotary joint, Doric Lenses) that allowed mice to freely move in the behavioural apparatus. Instead of directly manipulating dmPFC PNs, we capitalized on the properties of cortical PV<sup>+</sup> interneurons, which are a particular class of GABAergic interneurons regulating efficiently the output activity of cortical principal excitatory neurons<sup>30,31</sup>. Because a single PV<sup>+</sup> interneuron can contact more than 1,500 PNs<sup>32</sup>, the optogenetic activation or inhibition of population of  $PV^+$  represents an efficient tool for controlling PN activity  $^{14,33-35}$ . This strategy was motivated by the fact that optogenetic manipulation of PNs was associated with large artefacts, which prevented the simultaneous recording of LFPs (Extended Data Fig. 5c). For optogenetic manipulation of  $PV^+$  interneurons during behaviour, we used 30 ms light pulses delivered under specific behavioural and neurophysiological conditions (see section on 'Closed-loop stimulation'). After behavioural and recording experiments, mice were perfused and histological analysis was performed.

Anatomical and histological analysis. Mice were euthanized with isoflurane and perfused through the left ventricle with 4% w/v paraformaldehyde in 0.1 M PBS. Brains were dissected out and postfixed for 4h at 4°C in the same solution. Sections  $(60\,\mu m \ thick)$  were cut, mounted on gelatin-coated microscope slides and dried. Sections were stained with toluidine blue, dehydrated and mounted. Electrolytic lesions were identified with conventional transmission light microscopy. Only recordings with confirmed lesions in cingulate and prelimbic areas of dmPFC were included in our analyses. It is important to note that because the electrode bundles are manually fabricated in the laboratory and individual wires can be slightly displaced during insertion in the brain, the distance between each electrode cannot be measured precisely. It is therefore technically impossible to determine from which layer the single unit and LFP recorded from the same electrode were performed. For verification of viral injections in dmPFC (which include the cingulate cortex ACC and the prelimbic area), serial 80-µm-thick slices containing the dmPFC were imaged using an epifluorescence system (Leica DM 5000) fitted with a 10× dry objective. The location and the extent of the injections/infections were visually controlled. Only infections accurately targeted to dmPFC were considered for behavioural and electrophysiological analyses.

Single-unit analyses. Single-unit spike sorting was performed using Off-Line Sorter software (Plexon) for all behavioural sessions. Principal component scores were calculated for unsorted waveforms and plotted in a three-dimensional space defined by principal components and/or timing and voltage features of the waveforms; clusters containing similar valid waveforms were manually defined. A group of waveforms were considered to be generated from a single neuron if the waveforms formed a discrete, isolated, cluster in the three-dimensional space and did not contain a refractory period less than 1 ms, as assessed using inter-spike interval analysis. To avoid analysis of the same neuron recorded on different channels, we computed cross-correlation histograms. If a target neuron presented a peak of activity at a time that the reference neuron fired, only one of the two neurons was considered for further analysis. To separate putative inhibitory interneurons from putative excitatory PNs we used an unsupervised cluster algorithm based on Ward's method. In brief, the Euclidian distance was calculated between all neuron pairs on the basis of the three-dimensional space defined by each neuron's average half-spike width (measured from trough to peak), the firing rate and the area under the late positive deflection phase of the spike. An iterative agglomerative procedure was then used to combine neurons into groups based on the matrix of distances such that the total number of groups was reduced to return the smallest possible increase in within-group sum of square deviation. Cross-correlation analysis was then performed to evaluate the excitatory or inhibitory nature of each neuron on other simultaneously recorder units. To assess the significance of cross-correlogram analyses performed between pairs of recorded neurons, a mean firing rate with 95% confidence limits of the target neuron firing rate was calculated. Significant short-latency inhibitory or excitatory interactions were retained if the number of action potentials of the target neuron was inferior or superior to these 95% confidence limits, respectively. Note that among the clusters of PNs and interneurons, no PNs were found to inhibit another cell and no interneurons were found to excite another cell. To identify the main firing patterns among PNs, we used an unbiased principal component analysis based on the neuronal activity evoked by CS<sup>+</sup> presentations (z-score 500 ms before and after CS<sup>+</sup> presentations, CS<sup>+</sup> presentations one to four in the post-fear-conditioning sessions, each CS<sup>+</sup> consisting of 27 individual sound pips; bin size of 10 ms). Only the first principal component was considered (PC1) because it explained most of the variance of our data set. One neuron was excluded from analysis on the motive of an absence of spiking activity around the time of CS<sup>+</sup> presentation. Neurons (n=289) were classified as correlated, indifferent of inversely correlated with PC1 at the P < 0.05 significance level.

**Neuronal assembly isolation.** We hypothesized that single neurons of the dmPFC functionally aggregate into discrete assemblies to code for fear expression. We used a previously published method<sup>36</sup> to evaluate the possibility that a subset of PNs is coactivated during discrete time windows inside freezing epochs. We calculated single-unit rate histograms with a sliding window of 150 ms and 100 ms overlap, to minimize potential slicing of assembly realizations. In this study we were interested in identifying which neurons were coactivated rather than how much they were coactivated. We therefore focused on the sole presence or absence of activity for a neuron inside each time bin independently of its actual firing rate.

To this end, the rate histograms were binarized in such a way that any bin value strictly above zero was given a value of 1 (otherwise 0, Extended Data Fig. 3a, top). Binarized histograms for *n* simultaneously recorded PNs were then concatenated and we calculated the  $n \times n$  coactivation matrix of the PN population for each time bin (Extended Data Fig. 3a, bottom). To investigate the emergence of specific coactivation pattern during the recording session, principal component analysis was performed on the coactivation matrix. We considered only the score on the first principal component (PC1) that explains the greatest part of the coactivation matrix variance. To extract putative coactivation matrix pattern related to fear expression, we then analysed the distribution of PC1 scores as a function of animal freezing behaviour. Note that we also investigated the impact of sliding window length on PC1 score distributions inside and outside freezing epochs to define the optimal window length to isolate freezing-related neuronal assemblies. The optimal window length was found to be 150 ms, as shorter windows were not as efficient in discriminating freezing versus no-freezing epochs and larger windows were not further ameliorating that discrimination (Extended Data Fig. 3c). The probability of a certain PC1 score predicting freezing was analysed using a bootstrap method as follows. PC1 score was binned (0.1 units) and we calculated the freezing probability associated with each score bin. The same procedure was applied to a set of surrogate data for which freezing intervals were shuffled 50 times. Actual and surrogate freezing probabilities as a function of PC1 score were then compared to retrieve the threshold above which PC1 score predicted freezing behaviour above chance level (red dotted line in Extended Data Fig. 3b, d-e, h-m). This threshold was then used to isolate coactivation matrix patterns predicting freezing behaviour (hereafter named coactivation matrix freezing patterns). Finally, we identified and analysed which single neurons were coactive inside coactivation matrix freezing patterns associated with freezing behaviour (Extended Data Fig. 3f, top). Note that the weight of a neuron within the coactivation matrix freezing pattern can be solely due to its random probability of spiking (for example, neurons that increase firing during freezing would be more likely to co-fire). To correct for this potential bias, we tested the significance of each single neuron contribution to the coactivation matrix freezing pattern against that of a surrogate data set (50 time shuffling of the spike train inter-spike intervals, Extended Data Fig. 3f, bottom). The average coactivation matrix was normalized by dividing it by the average surrogate coactivation matrix (Fig. 1e, all other examples see Extended Data Fig. 3h-m). Each neuron was then given an assembly participation index (AP index) defined as the ratio between its average and surrogate firing rates for coactivation matrix freezing patterns (Fig. 1d, e). Each neuron displaying an AP index significantly above the chance level (chance: AP index = 1) defined by the confidence interval of surrogate data was considered as an AN (AP index > 1). Units with an AP index inferior or equal to chance level were classified as ONs (ON, AP index < 1).

LFP analyses. LFPs were analysed using custom scripts from Matlab, as well as an open source Matlab toolbox for the analysis of circular statistics<sup>37</sup>. LFP signals were filtered in the 4 Hz range (3-6 Hz) using a second-order Butterworth filter. To evaluate 4 Hz phase locking of individual neurons, we calculated the instantaneous phase of the 3–6 Hz filtered LFPs using the Hilbert transform. For a given neuron, each spike was assigned its corresponding LFP 4 Hz phase value from the LFP signal recorded on the same wire. Phase locking was calculated using Rayleigh's test for circular uniformity and statistical significance was assessed using Rayleigh's test P and z values. For significantly phased-locked PNs, we quantified the preferred phase as well as phase locking strength using the MRL. Importantly, MRL estimate is highly dependent on the sample size. To account for this bias, we computed MRL only for significantly phase-locked neurons displaying at least 50 spikes. Therefore, at least the relative comparisons of 4 Hz modulation strength between conditions should not be affected by sample sizes (number of spikes). For time-frequency analysis, we used wavelet decomposition of LFP signals. LFPs were convolved by a family of Morlet's wavelets, one for each frequency between 2 and 16 Hz (with a log<sub>2</sub> scale) as a function of time. Power spectral density for freezing and non-freezing epochs was retrieved by averaging the results of the time-resolved wavelet analysis across those specific time intervals. To average LFP power across animals, we first normalized the power spectral density histogram as the percentage of total power between 2 and 16 Hz. To compare  $\theta$  (8–12 Hz) and 4 Hz frequencies in freezing and non-freezing epochs we calculated the 4 Hz to  $\theta$  ratio:

$$\frac{\sum PSD_{4Hz} - \sum PSD_{\theta}}{\sum PSD_{4Hz} + \sum PSD_{\theta}}$$

We addressed the correlation in time between freezing episode onset and offset and LFP oscillations in the 2–16 Hz frequency range by calculating the average peri-event time spectrograms of dmPFC LFP around the onset or offset of freezing epochs. We then addressed the putative relationship between neuronal assembly occurrence and the modulation of certain frequency components in the LFP at the time of freezing onset and offset. For this we computed a linear correlation between

assembly rate (occurrence per second) and LFP power at each frequency between 2 and 16 Hz. To assess 4 Hz and assembly dynamics inside freezing and no freezing episodes, we normalized the length of freezing and no-freezing intervals to express time as the percentage of time elapsed inside each interval.

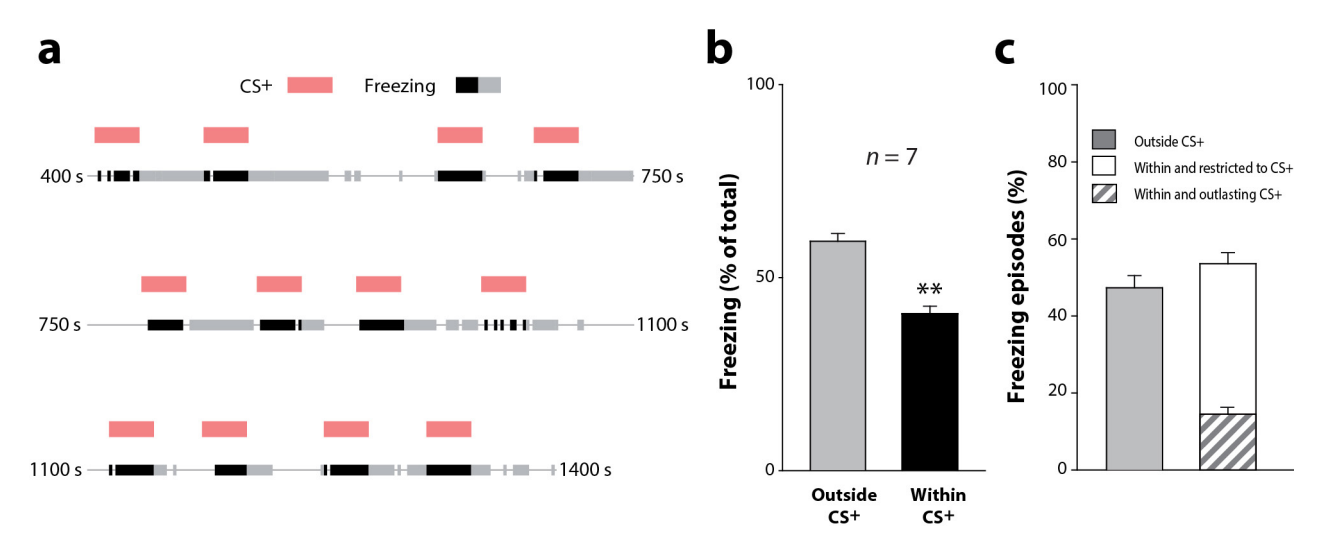
To evaluate the average pairwise co-firing between pairs of PN as a function of 4 Hz phase, spike trains were binned according to LFP 4-Hz phase (36° bin size), and for each bin class the pairwise co-firing index was calculated as the ratio of co-occurring (common) spikes to the total number of spikes in the bin class for the two units. This provides a simple yet direct measure of the co-occurrence of unit spikes as a function of phase. To ensure the pairwise co-firing of AN neurons was not artificially enhanced by (1) the temporal relation between pairs of AN neurons or (2) the cycle-to-cycle relation between AN neurons (phase relation), we computed a shuffled co-firing (1) and phase-shift predictor (2) as follows. For the shuffled co-firing analysis, for each pair of PNs, one spike train inter-spike intervals were time-shuffled 50 times and the mean surrogate co-firing for each phase bin value recalculated. We then averaged over all AN or ON neuron pairs. This analysis conserves the overall firing rate of the shuffled spike train but destroys the temporal relationship between the two spike trains. Since ANs and ONs present different firing rates and different modulations of firing rates in relation to freezing (Extended Data Fig. 4a), this correction allows the comparison of co-firing between both populations. For the shift predictor analysis, for each 36° phase bin and each pair of AN neurons, 4Hz cycles were given an index from 1 to n, n corresponding to the total number of 4 Hz cycles in the recording. Indices were then shuffled 50 times for the reference neuron and the mean surrogate co-firing was calculated. This analysis destroys the cycle-to-cycle relation between the two spike trains while preserving the firing modulation by behaviour. We then calculated the corrected pairwise co-firing by subtracting both the shuffled co-firing and the shift predictor to the actual co-firing and subsequently evaluated the sole contribution of freezing or phase to the co-firing of PN. In addition we assessed the impact of the instantaneous power of 4 Hz oscillations on PN co-firing. To this end we calculated pairwise co-firing as a function of phase for different classes of 4 Hz power. Power during freezing was z-scored and binned (0.49 s.d.) and pairwise co-firing was calculated as a function of phase and power. The analysis was restricted to the -1.96 s.d. to +1.96 s.d. power range (eight bins) encompassing 95% of power values to exclude extreme values with low occurrence. To compare ANs and ONs on the way their phase-specific pairwise co-firing is impacted by 4 Hz power change, we calculated the difference in corrected co-firing between ascending and descending phases as follows:  $\Delta CF = max(CF_{ascending})/min(CF_{descending})$ .

Closed-loop stimulation. Neurons forming a functional assembly cannot be specifically manipulated using a standard optogenetic approach. Although such cellular specificity is unattainable to this day, a certain temporal specificity exists as the activation of fear coding neuronal assemblies is specific of 4 Hz ascending phase. To apply our stimulation in a functionally specific manner, we performed optogenetic inhibition of PNs as a function of the phase (ascending or descending) of the ongoing 4 Hz oscillation in dmPFC LFP. To that end we designed a closed-loop stimulation protocol where animal behaviour (freezing) and dmPFC LFP (4 Hz power and phase) were monitored online and simultaneously analysed to drive a laser beam. Animal position was sampled at 80 Hz and LFP at 1 KHz, then uploaded every 10 ms in Matlab for online analysis. The former served, on the one hand, to quantify animal speed in the last 1,000 ms of uploaded signal and on the other hand to bandpass filter the LFP signal (3–6 Hz range) and retrieve both 4 Hz power in the last 500 ms and 4 Hz phase for the last recorded data point.

Animal speed was calculated as the average distance travelled over the last 1,000 ms time window and compared with the freezing threshold. Bandpass filtering was applied using a second-order Butterworth filter and Hilbert transform was used to estimate both 4 Hz power in the last 500 ms and LFP instantaneous phase for the last data point. Three conditions were defined for the stimulation. For the most recent 10 ms upload if (1) animal speed was below freezing threshold, (2) 4 Hz power was above that of baseline level and (3) 4 Hz phase was encompassed within the range of choice (ascending, 0–180°; or descending, 180–360°), then stimulation was triggered. The stimulation consisted of a 1 ms pulse sent from Matlab to a pulse generator (Master 9, AMPI) that in turn sent a 30 ms pulse to a blue/yellow laser generator to deliver optical stimulation to the dmPFC. The whole computation from neuronal data read to laser onset was achieved in 30 ms maximum (data retrieval 10 ms; computation 5–20 ms). Hence, at the end of the 30 ms light pulse, a new analysis loop was completed and if the three conditions were again fulfilled in the most recent 10 ms upload then a new stimulation pulse was triggered.

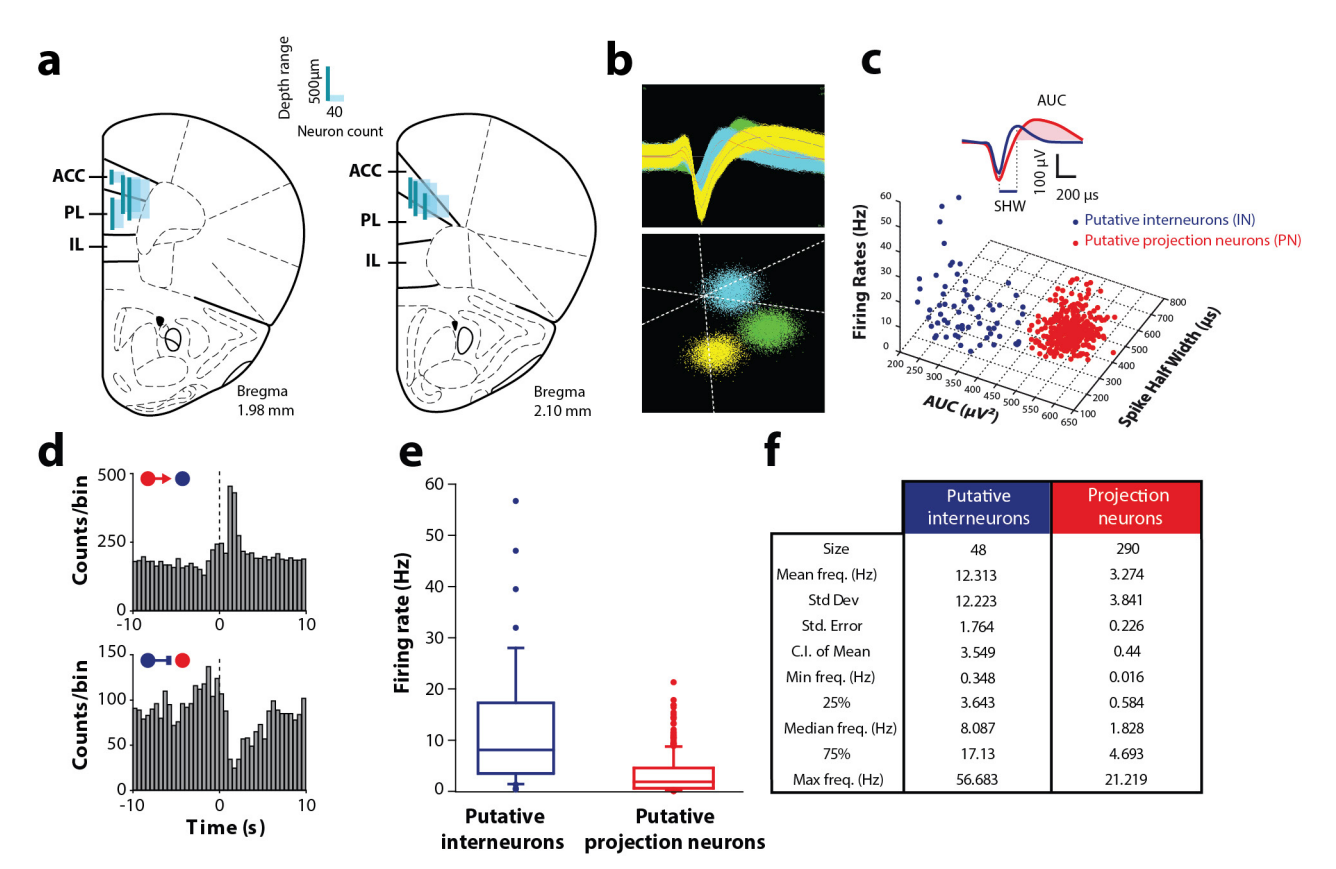
Statistical analyses. For each statistical analysis provided in the manuscript, the Kolmogorov-Smirnov normality test was first performed on the data to determine whether parametric or non-parametric tests were required. Two different approaches were used to calculate the sample size. For studies in which we had sufficient information on response variables, power analyses were performed to determine the number of mice needed. For studies in which the behavioural effect of the manipulation could not be pre-specified, such as optogenetic experiments, we used a sequential stopping rule. In essence this method enables null-hypothesis tests to be used in sequential stages, by analysing the data at several experimental points using *t*-tests. Usually the experiment started by testing only a few animals and if the P value was below 0.05, the investigator declared the effect significant and stopped testing. If the P value was greater than 0.36, the investigator stopped the experiment and retained the null hypothesis. For sample size estimation using power analyses, we used an online power analysis calculator (G\*power 3). For each analysis, sample size was determined using a power > 0.9 and alpha error = 0.05. All tests were two sided. Sample size determination using sequential stopping rule analyses were used for optogenetic experiments in which it was not possible to determine a priori the effect of the optical manipulation. We used P values of 0.05 and 0.36 for lower and upper criteria. Using this strategy, we ended up with a value of *n* comprising between five and seven animals per group. No randomization or investigator blinding was done.

- 30. Markram, H. et al. Interneurons of the neocortical inhibitory system. Nature Rev. Neurosci. 5, 793–807 (2004).
- Somogyi, P., Freund, T. F. & Cowey, A. The axo-axonic interneuron in the cerebral cortex of the rat, cat and monkey. Neuroscience 7, 2577–2607 (1982).
- Sik, A., Penttonen, M., Ylinen, A. & Buzsáki, G. Hippocampal CA1 interneurons: an in vivo intracellular labeling study. J. Neurosci. 15, 6651–6665 (1995).
- Kvitsiani, D. et al. Distinct behavioural and network correlates of two interneuron types in prefrontal cortex. Nature 498, 363–366 (2013).
- Wolff, S. B. et al. Amygdala interneuron subtypes control fear learning through disinhibition. Nature 509, 453–458 (2014).
- 35. Stark, E. et al. Inhibition-induced theta resonance in cortical circuits. *Neuron* **80**, 1263–1276 (2013).
- Peyrache, A., Benchenane, K., Khamassi, M., Wiener, S. I. & Battaglia, F. P. Principal component analysis of ensemble recordings reveals cell assemblies at high temporal resolution. J. Comput. Neurosci. 29, 309–325 (2010).
- Berens, P. CircStat: a MATLAB toolbox for circular statistics. J. Stat. Softw. 31, 1–21 (2009).



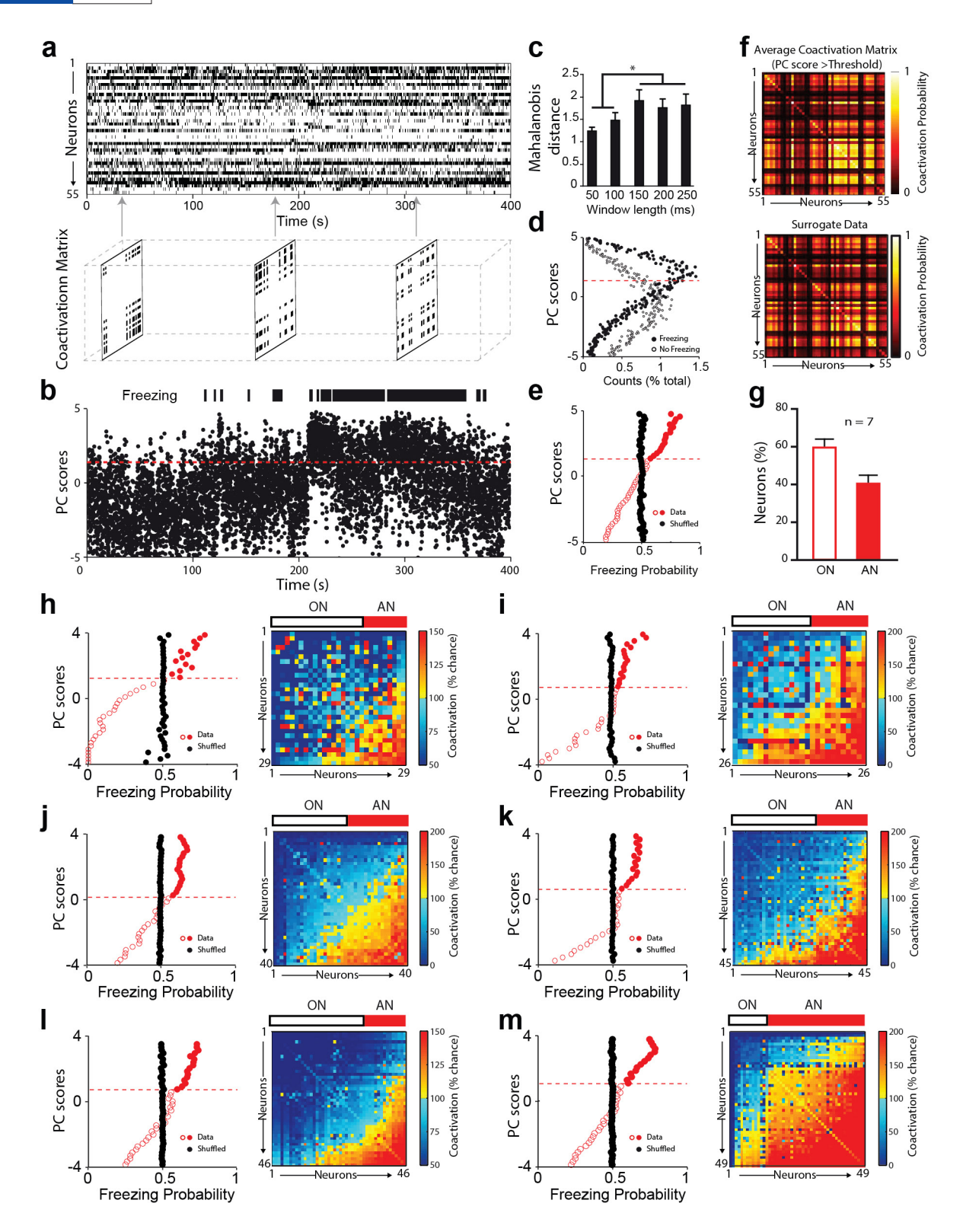
Extended Data Figure 1 | CS $^+$ -triggered and spontaneous occurrence of conditioned freezing responses. a, Representative examples of conditioned freezing behaviour periods recorded 24 h after auditory fear conditioning (post-FC session). Freezing epochs occurred either independently of any sensory stimulation (thick grey lines) or were induced by CS $^+$  presentations (thick black lines). b, Averaged percentage

of freezing behaviour recorded 24 h after auditory fear conditioning (post-FC session) within or outside CS<sup>+</sup> presentations (n=7 mice, paired t-test, within versus outside CS<sup>+</sup>, \*\*P < 0.01). c, Averaged percentage of freezing episodes initiated outside or within CS<sup>+</sup> presentations and restricted or outlasting CS<sup>+</sup> presentations (n=7 mice). Error bars, mean  $\pm$  s.e.m.



**Extended Data Figure 2** | **Separation of putative PNs and putative interneurons. a**, Location and depth of recording sites in the dmPFC and number of neurons recorded (n=7 mice). **b**, Top: superimposed waveforms recorded from three different units. Bottom: spikes originating from individual units were sorted using three-dimensional principal component analysis. **c**, Among the population of neurons recorded, 86% were classified as putative projection neurons (PN, red circles, n=290) and 14% as putative interneurons (IN, blue circles, n=48) using an unbiased unsupervised cluster separation algorithm based on three electrophysiological properties: firing frequency, spike half width (SHW) and spike area under waveform peak. Inset, average waveform of a representative PN and interneuron illustrating the methodology used to quantify SHW and the spike segment used to calculate the spike area under waveform. **d**, Top: representative cross-correlogram performed

between a PN and interneuron showing a short-latency, presumably monosynaptic, excitatory interaction (no inhibitory interaction identified among all significant cross-correlograms identified). Bottom: representative cross-correlogram between an interneuron and a PN showing a short-latency, possibly monosynaptic, inhibitory interaction (no excitatory interaction identified among all significant cross-correlograms identified). Reference events correspond to the spikes of the presynaptic neuron (dashed line at time 0, bins of 0.5 ms). Red and blue circles represent PNs and interneurons, respectively. **e**, Box plot of the firing rate of PNs (n=290 in 7 mice) and interneurons (n=48 in 7 mice). For each box plot, the middle, bottom and top lines correspond to the median, lower quartile and upper quartile firing rates. Blue and red dots below and above the boxes correspond to outlier data points. **f**, Corresponding firing frequency statistics for PNs and interneurons.

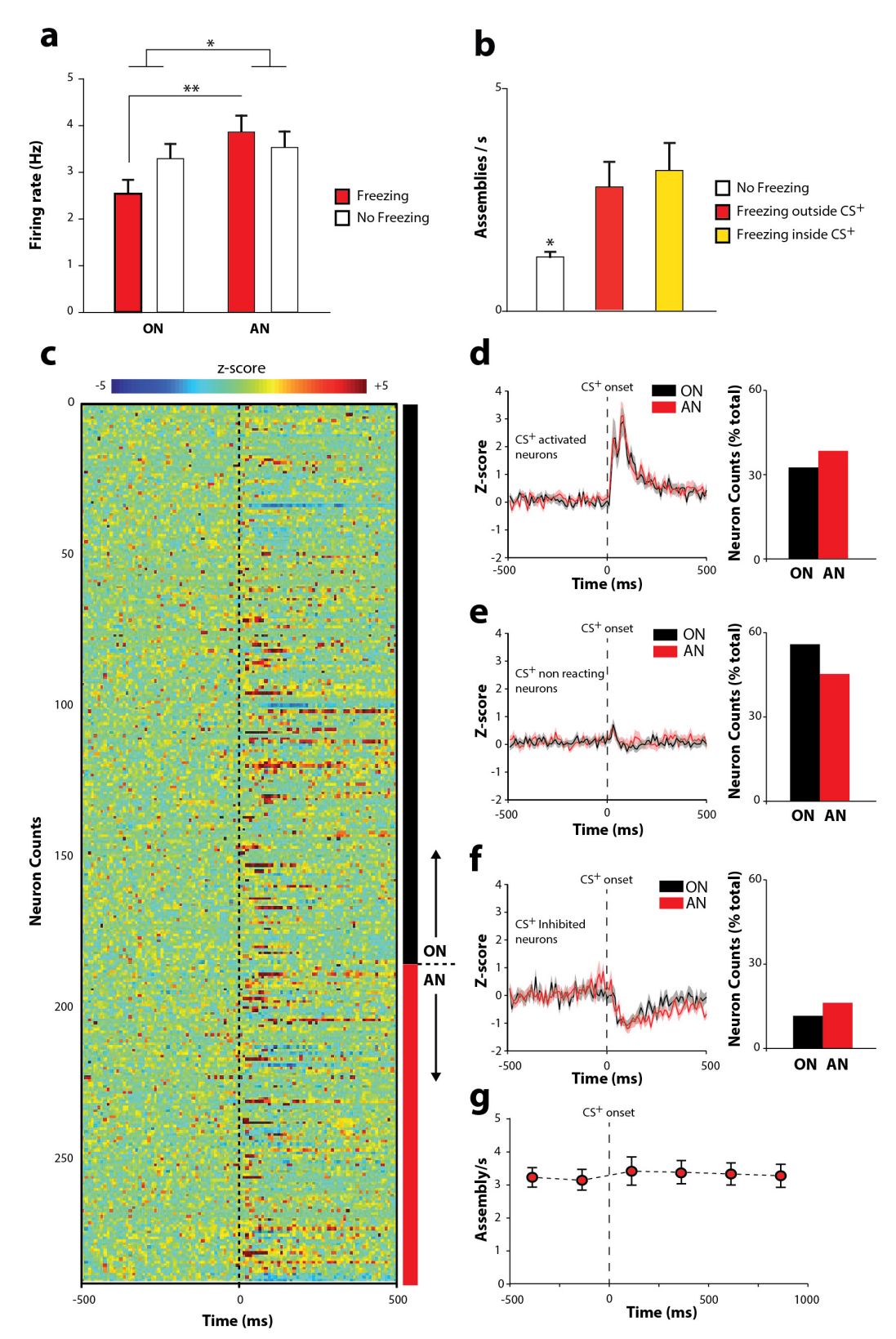


Extended Data Figure 3 | See next page for caption.

Extended Data Figure 3 | Isolation of dmPFC neuronal assemblies.

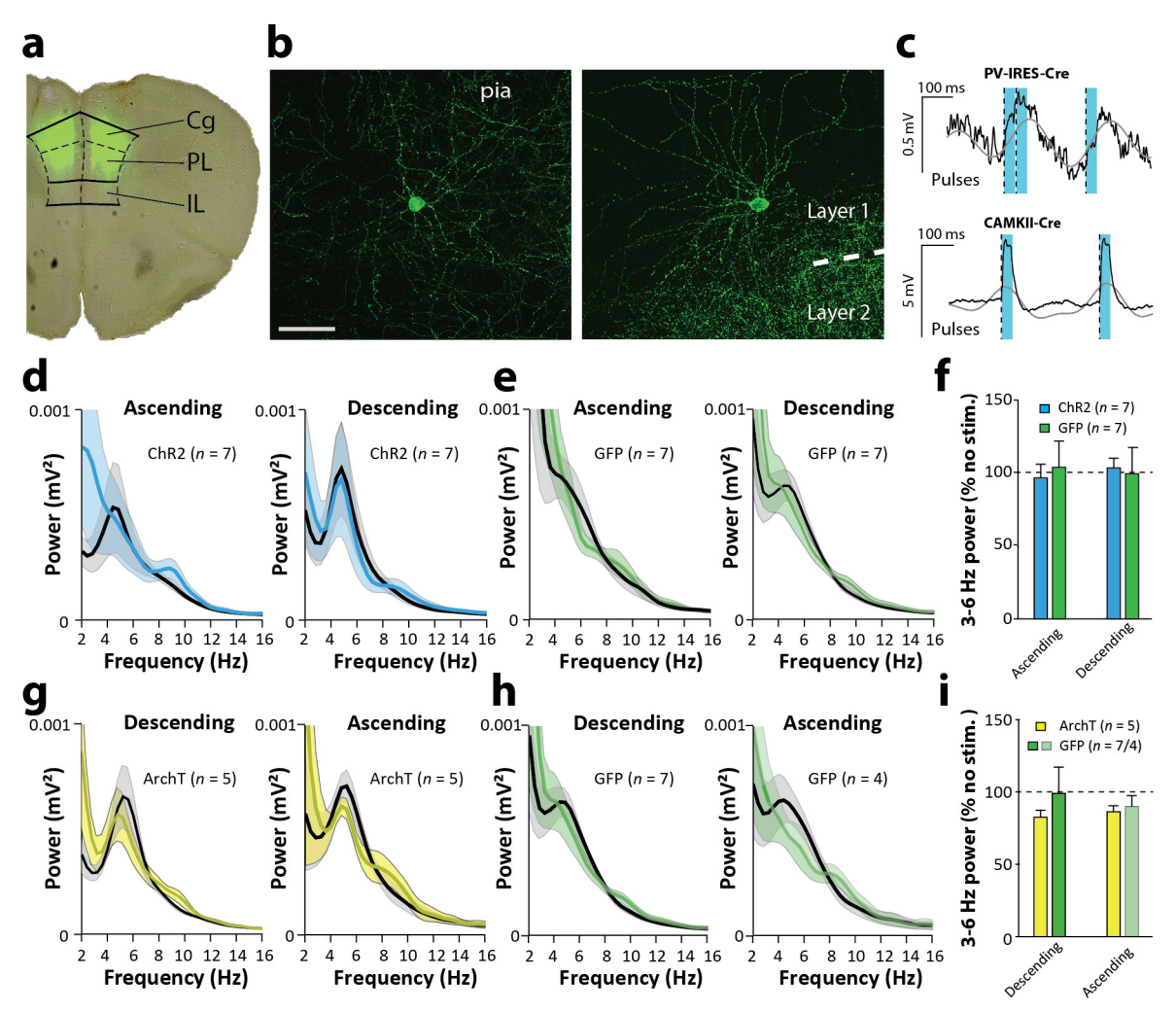
a, Top: example of a binarized rate histogram matrix computed from 55 PNs recorded in a single animal. Bottom: examples of correlation matrices computed for particular time bins from the same 55 PNs (bin size: 150 ms). b, Corresponding example of principal component scores for the same population of 55 PNs and freezing behaviour as a function of time. For the displayed component (first principal component), the distribution of scores is different for freezing and no freezing periods. This shows that freezing episodes are associated with a specific profile of activity for the simultaneously recorded neurons taken as a population. c, Averaged Mahalanobis distance between neuronal population profiles correlated with freezing and no freezing epochs as a function of the length of the sliding window used to produce the binarized rate histograms (see Methods). The optimal separation for neuronal population profiles correlated with freezing and no freezing epochs was obtained with sliding window lengths between 150 and 250 ms (n = 7 mice, Friedman repeated-measures one-way ANOVA on ranks test, \*P < 0.05). Error bars, mean  $\pm$  s.e.m. **d**, Corresponding example distribution of principal component scores for neuronal population profiles correlated with freezing (black dots) and no freezing (white dots) epochs (Wilcoxon signed rank test, P < 0.05). e, Corresponding example of freezing probability as a function of neuronal population principal component score. Freezing probability associated with each score is compared with

surrogate data (black dots) for which freezing intervals have been shuffled. Plain and open red dots represent neuronal population profiles that are significantly over-represented compared with chance during freezing and no freezing periods, respectively (one sample *t*-test, surrogate data versus actual freezing probability for each score, for scores equal to or above 1.15, freezing probability superior to chance level and P < 0.05). The red dotted line represents the boundary between neuronal population profiles correlated with freezing and no freezing epochs. f, Top: coactivation matrix averaged over freezing epochs from the same 55 dmPFC PNs recorded in a single animal. The strength of the coactivation between pairs of neurons is expressed as the percentage of coactivation compared with chance. Bottom: surrogate data. Coactivation matrix averaged over freezing epochs from the same 55 dmPFC PNs recorded in a single animal for which spike trains have been shuffled 50 times. g, Average percentage of ANs (AP index > 1) and ONs (AP index < 1) to freezing-activated neuronal assemblies (n = 7 mice, ON: 59.6  $\pm$  4.5%; AN: 40.4  $\pm$  4.5%). h−m, Left: example of freezing probability as a function of neuronal population principal component score for individual mice as in e. Right: normalized coactivation matrix averaged over freezing predicting epochs from dmPFC PNs recorded in individual animals (n = 29, 40, 46, 26, 45and 49 neurons). The strength of the coactivation between pairs of neuron is expressed as the percentage of coactivation compared with chance. Error bars, mean  $\pm$  s.e.m.



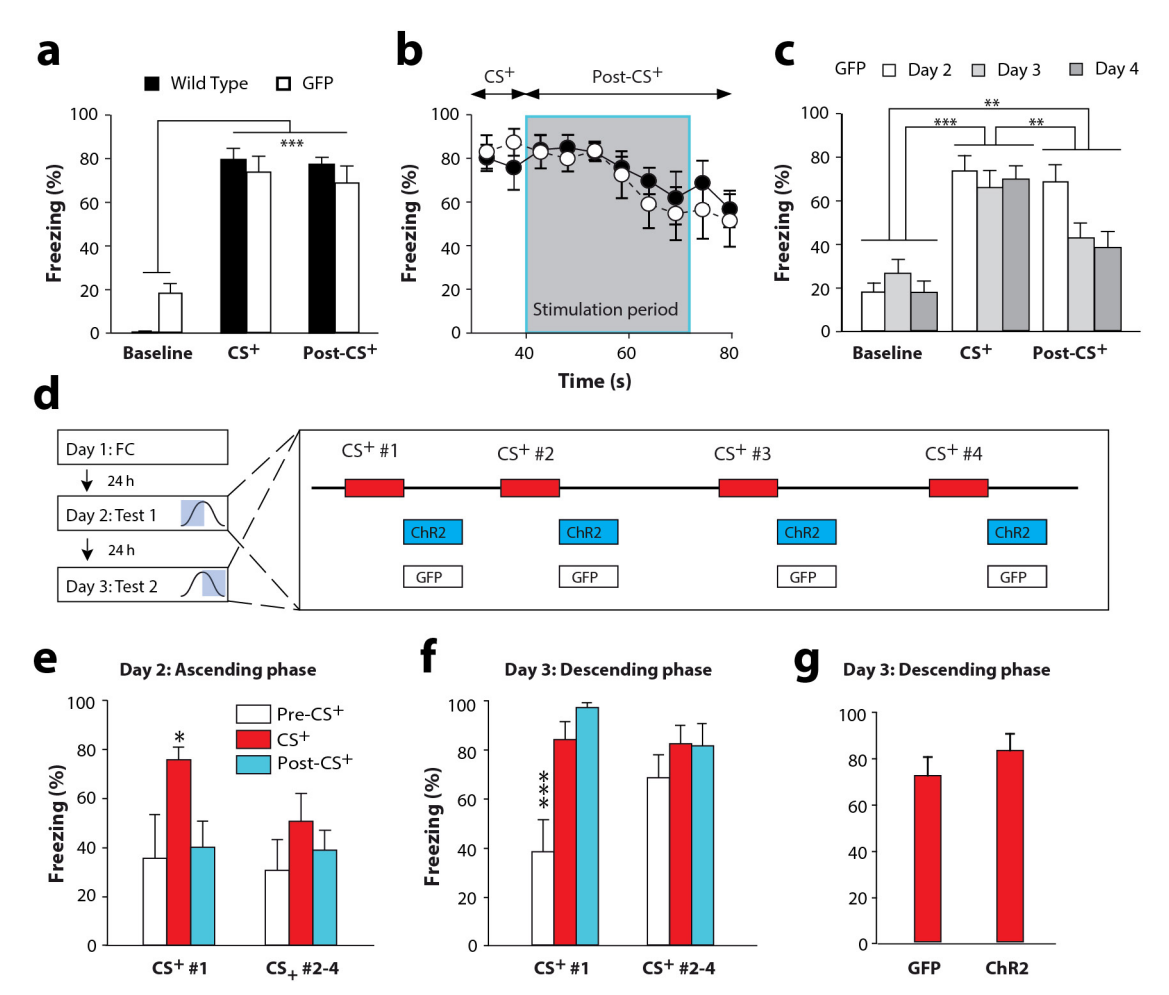
**Extended Data Figure 4** | CS<sup>+</sup>-evoked firing activity of dmPFC PNs. **a**, Averaged firing rate during freezing and no freezing periods for ANs and ONs (n=7 mice, two-way ANOVA, factor 1: AN versus ON, P<0.05; factor 2: freezing versus no freezing, P>0.05;  $F_1\times F_2$ : P>0.05; Student–Newman–Keuls post-hoc test within freezing, \*\*P<0.01, \*P<0.05). **b**, Average neuronal assembly rate during no freezing periods and during freezing episodes within or outside CS<sup>+</sup> presentations (n=7 mice, Friedman repeated-measures one-way ANOVA on ranks test, no freezing versus freezing (inside or outside CS<sup>+</sup>), P<0.05; Student–Newman–Keuls post-hoc test, \*P<0.05). **c**, Z-score-normalized

peri-stimulus time histograms of individual dmPFC ANs (n=117) and ONs (n=172) during freezing episodes. **d-f**, Left: mean z-score of CS<sup>+</sup>-evoked significant excitatory (**d**), unchanged (**e**) or significant inhibited (**f**) neuronal responses for dmPFC AN and ON. Grey and pink shaded areas correspond to mean  $\pm$  s.e.m. Right: corresponding percentage of AN and ON (n=7 mice,  $\chi^2$  test, P>0.05 in all cases; CS<sup>+</sup>-evoked excitation: AN: 38.5%, ON: 32.6%; CS<sup>+</sup>-evoked no changes: AN: 45.3%, ON: 55.8%; CS<sup>+</sup>-evoked inhibition: AN: 16.2%, ON: 11.6%). **g**, The probability of observing assembly activation is not affected by CS<sup>+</sup> (repeated-measures one-way ANOVA on ranks, P>0.05). Error bars, mean  $\pm$  s.e.m.



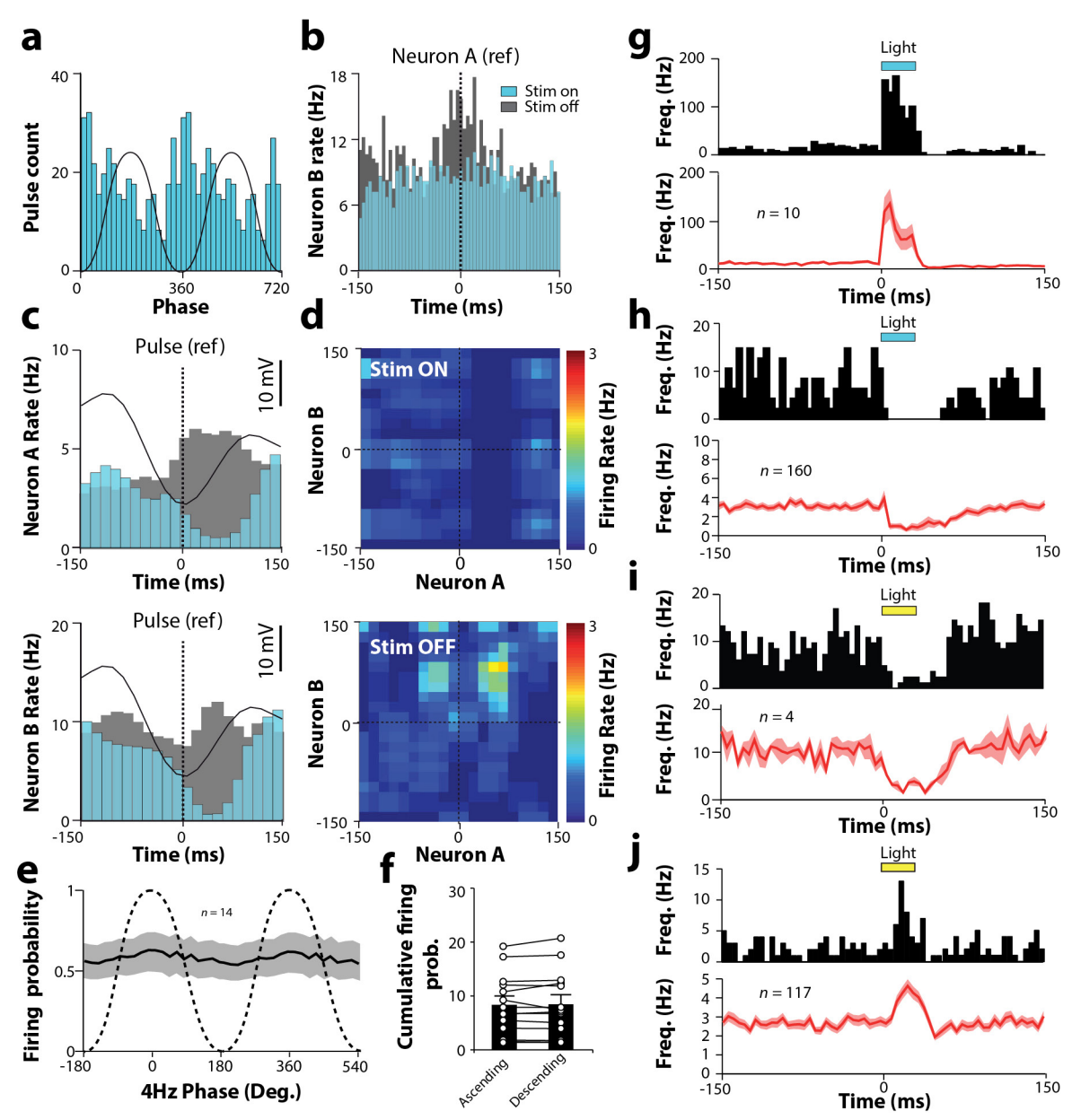
Extended Data Figure 5 | Histological controls and closed-loop stimulation technique. a, Representative micrograph used for dmPFC GFP expression assessment. **b**, Representative dmPFC PV interneurons with distinct dendritic arborizations were infected. Left: multipolar neuron with a round soma, corresponding to a putative basket cell. Right: interneuron with an ovoid soma at the layer 1-2 border, displaying asymmetric and tufted dendrites. Some branches extend towards the pia, bend and follow the pial surface. This neuron corresponds to the typical description of axo-axonic (chandelier) cells in mPFC. c, Top: representative raw (black trace) and filtered (grey trace, 3-6 Hz) dmPFC LFP recorded in PV-IRES-Cre mice during 4 Hz oscillations (top) or in CAMKII-Cre mice outside 4 Hz oscillations infected with ChR2 (bottom) upon light activation (30 ms square pulses; black line, pulse start; red bar, pulse length). d, e, Averaged LFP power spectra obtained in ChR2-infected mice and GFP controls during stimulated (coloured traces) and nonstimulated (grey traces) periods when the stimulation was applied in the

ascending (ChR2, n = 7 mice; GFP, n = 7 mice) or descending (ChR2, n = 7mice; GFP, n = 7 mice) phase. f, Averaged 3–6 Hz LFP power for ChR2 and GFP mice during stimulation in the ascending or descending phase of 4 Hz oscillations expressed as a percentage of no stimulation periods (ChR2, n = 7 mice; GFP, n = 7 mice; two-way ANOVA, factor 1: GFP versus ChR2, P = 0.848; factor 2: descending versus ascending, P = 0.879;  $F_1 \times F_2$ , P = 0.618). **g**, **h**, Averaged LFP power spectra obtained in ArchT infected mice and GFP controls during stimulated (coloured traces) and non-stimulated (grey traces) periods when the stimulation was applied in the descending (ArchT, n = 5 mice; GFP, n = 7 mice) or ascending phase (ChR2, n = 5 mice; GFP, n = 4 mice). i, Averaged 3–6 Hz LFP power for ArchT and GFP mice during stimulation in the descending or ascending phase of 4 Hz oscillations expressed as a percentage of no stimulation periods (ArchT, n = 5 mice; GFP, n = 7/4 mice; two-way ANOVA, factor 1: GFP versus ChR2, P = 0.872; factor 2: descending versus ascending, P = 0.183;  $F_1 \times F_2$ , P = 0.5). Error bars, mean  $\pm$  s.e.m.



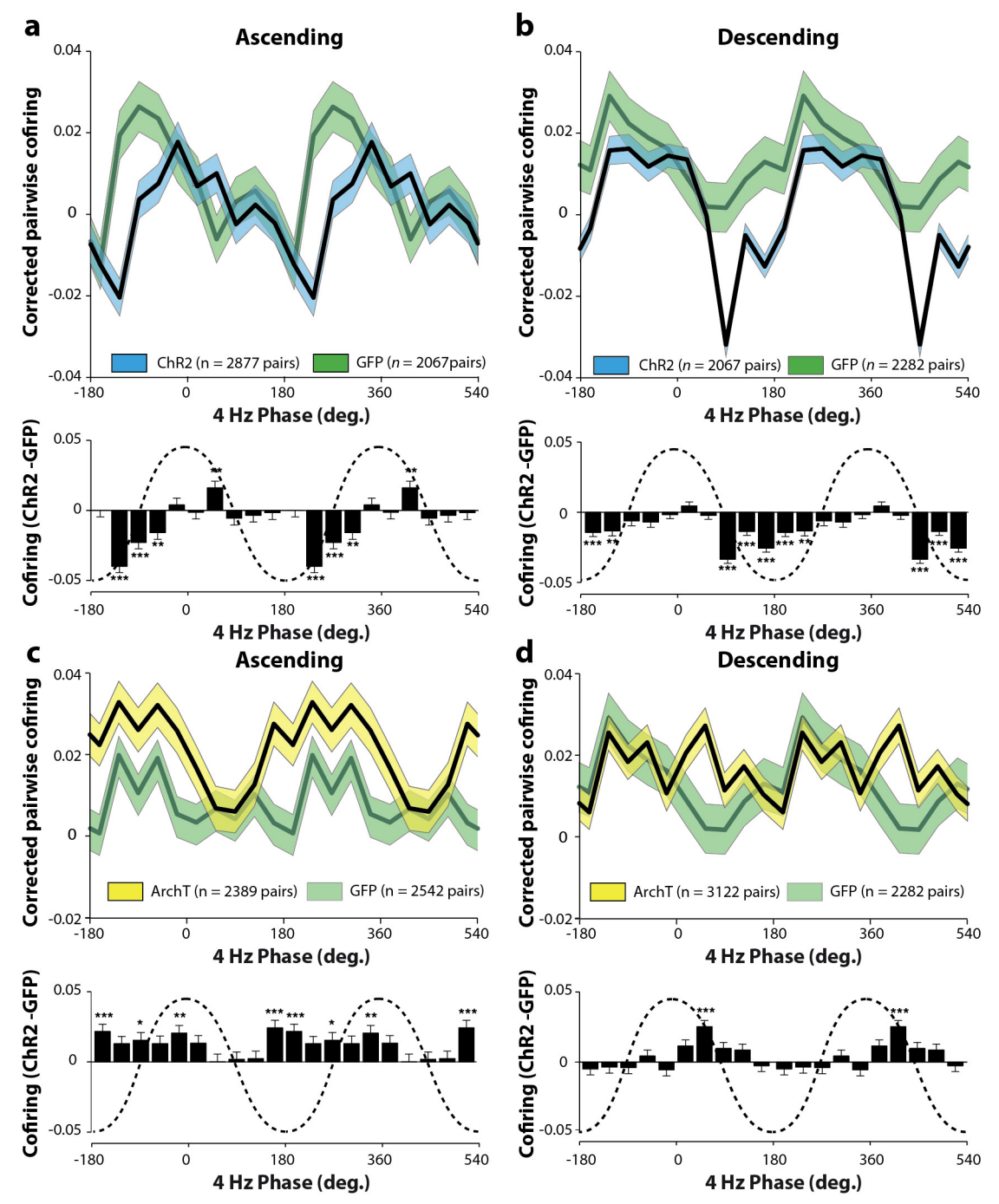
Extended Data Figure 6 | Phase-specific optogenetic inhibition of dmPFC PNs. a, Twenty-four hours after conditioning, levels of freezing in wild type (n = 7) and GFP (n = 7) control animals where similar (2 min baseline, four CS<sup>+</sup> and four post-CS<sup>+</sup> periods of 30 s averaged, two-way ANOVA, factor 1: wild type versus GFP, P > 0.05; factor 2: time, P < 0.001;  $F_1 \times F_2$ , P < 0.01, Student–Newman–Keuls post-hoc test within wild type and GFP, \*\*\*P < 0.001). **b**, Corresponding time-resolved changes in freezing behaviour around CS<sup>+</sup> offset for wild type and GFP control animals (two-way ANOVA, factor 1: wild type versus GFP, P > 0.05; factor 2: time, P > 0.05;  $F_1 \times F_2$ , P > 0.05). **c**, Comparison of GFP control levels of freezing during (CS<sup>+</sup>) and 30 s after CS<sup>+</sup> (post-CS<sup>+</sup>) on days 2 (n=7), 3 (n=7) and 4 (n=4) (2 min baseline, four CS<sup>+</sup> and four post-CS<sup>+</sup> periods of 30 s averaged; two-way ANOVA, factor 1: day, P > 0.05; factor 2: time, P < 0.001;  $F_1 \times F_2$ , P > 0.05; Bonferroni post-hoc test between epochs, \*\*P < 0.01, \*\*\*P < 0.001). **d**, Timeline scheme for the optogenetic stimulation protocol on day 2 with stimulation targeting the ascending phase of 4 Hz oscillation cycle (top) and day 3 with stimulation targeting the descending phase of 4 Hz oscillation cycle (bottom). e, f, Comparison of freezing levels between CS<sup>+</sup> 1 and CS<sup>+</sup> 2-4

for epochs 10 s preceding, during and 30 s after CS<sup>+</sup> during optogenetic stimulation (pre-CS<sup>+</sup>, CS<sup>+</sup> and post-CS<sup>+</sup> respectively) on day 2 (e) and day 3 (f). On day 2, ascending phase stimulation after CS<sup>+</sup> 1 induced a decrease of freezing levels during subsequent CS<sup>+</sup> epochs as no more difference was observed between pre CS<sup>+</sup>, CS<sup>+</sup> and post CS<sup>+</sup> for  $CS^+$  2–4 compared with  $CS^+$  1 (n=7 mice, repeated-measures two-way ANOVA, factor 1: CS<sup>+</sup> 1 versus CS<sup>+</sup> 2-4, P > 0.05; factor 2: epoch, P < 0.05;  $F_1 \times F_2$ , P > 0.05; Student-Newman-Keuls post-hoc test within factor 1, \*P < 0.05 compared with both pre- and post-CS<sup>+</sup> epochs). On day 3, descending phase stimulation after CS<sup>+</sup> 1 induced an increase in freezing levels during pre-CS+ epochs as no more difference was observed between pre-CS<sup>+</sup>, CS<sup>+</sup> and post-CS<sup>+</sup> for CS<sup>+</sup> 2-4 compared with CS<sup>+</sup> 1  $(n = 7 \text{ mice}, \text{ repeated-measures two-way ANOVA}, \text{ factor } 1: \text{CS}^+ \text{ 1 versus})$ CS<sup>+</sup> 2–4, P > 0.05; factor 2: epoch, P < 0.05;  $F_1 \times F_2$ , P < 0.05; Student– Newman–Keuls post-hoc test within factor 1, \*P < 0.001 compared with both CS<sup>+</sup> and post-CS<sup>+</sup> epochs). **g**, Averaged freezing behaviour evoked by CS<sup>+</sup> 1 presentation on day 3 if day 2 stimulation was in the ascending phase (GFP n = 7, ChR2 with day 2 ascending n = 7, Mann–Whitney rank sum test, P = 0.259).



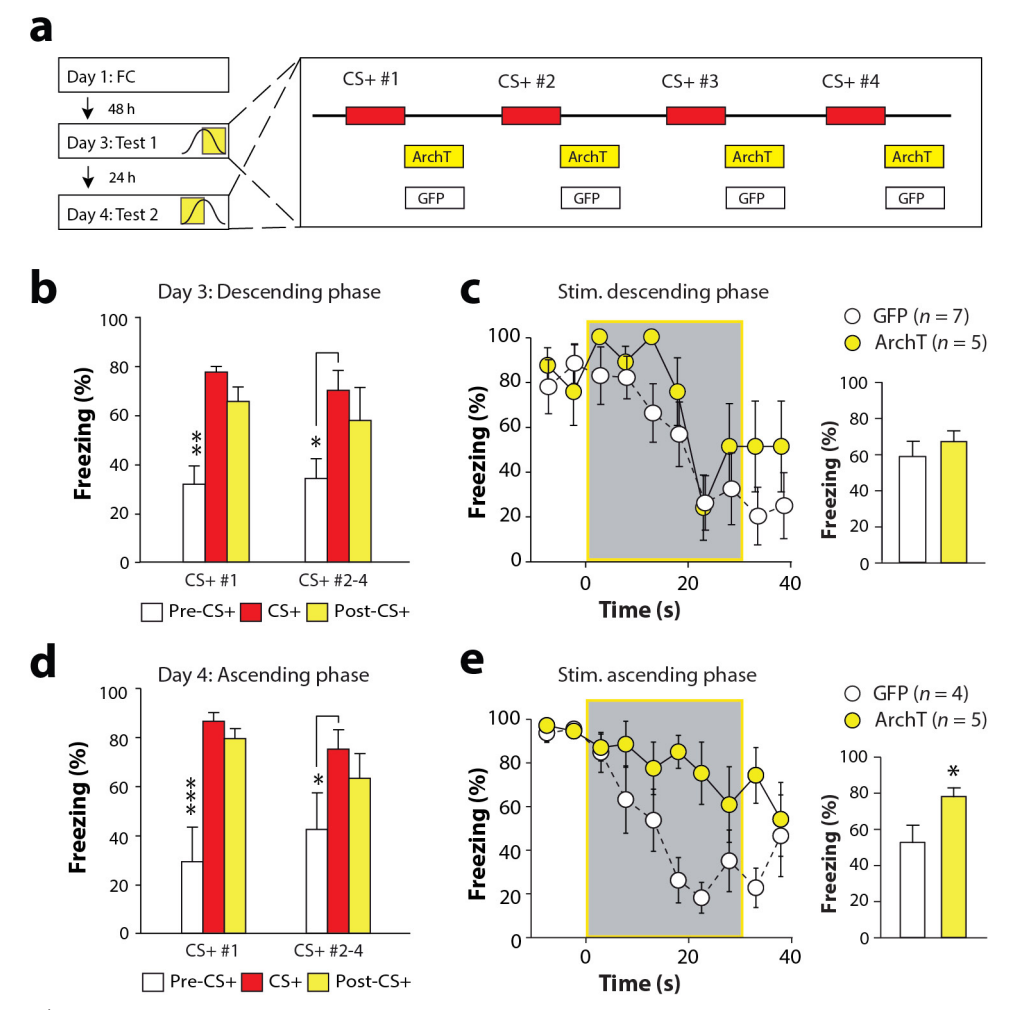
Extended Data Figure 7 | Phase specificity of the close loop stimulation technique. a, Representative distribution of stimulation pulses in relation to the phase of the 4 Hz oscillation (black line, filtered LFP 3-6 Hz) when the stimulation was applied in the ascending phase of the oscillation (bins of 18°). b, Representative cross-correlogram between two dmPFC PNs (neurons A and B) participating to neuronal assemblies during (blue bars), or outside (grey bars) optogenetic inhibition of PV interneurons. Note the reduction in joint firing activity when the stimulation was on. Reference events correspond to the spikes of the neuron A (dashed line at time 0, bins of 5 ms). c, Firing frequency of dmPFC neurons A (top) and B (bottom) without optogenetic stimulation (grey bars, bins of 15 ms) or when the pulse was applied in the ascending phase of the 4 Hz oscillation (blue bars, bins of 15 ms) (black line, filtered LFP 3-6 Hz). d, Corresponding joint peri-stimulus time histograms performed between the same dmPFC neurons A and B when the pulse was applied in the ascending phase of the 4 Hz oscillation (top) or without stimulation (bottom). Note the inhibition of the co-firing activity when the stimulation was on. e, Firing probability per degree of identified PV<sup>+</sup> interneurons as a function of

4 Hz oscillations phase ( $n = 14 \text{ PV}^+$  interneurons). **f**, Cumulative firing probability per degree for individual PV<sup>+</sup> interneurons (open circles) during the ascending or descending phase of 4 Hz oscillations and corresponding averaged cumulative firing probability (black bars, n = 14 $PV^+$  interneurons, Wilcoxon signed rank test, P = 0.733). g, i, Top: firing of a PV<sup>+</sup> interneuron in a mouse expressing ChR2 or ArchT in PV<sup>-</sup> interneurons in the dmPFC in response to blue or yellow light (light-pulse duration 30 ms; 150 trials). Bottom: mean peri-stimulus time histograms of all PV<sup>+</sup> interneurons displaying significant light-evoked excitation or inhibition ( $n = 10 \text{ PV}^+$  from five mice infected with ChR2;  $n = 4 \text{ PV}^$ from two mice infected with ArchT, light-pulse duration, 30 ms). Bins of 5 ms. h, j, Top: firing of a PN in a mouse expressing ChR2 or ArchT in PV<sup>+</sup> interneurons in the dmPFC in response to blue or yellow light activation of PV<sup>+</sup> interneurons (light-pulse duration, 30 ms; 150 trials). Bottom: mean peri-stimulus time histograms of all PNs displaying significant lightevoked inhibition or excitation (n = 160 PNs from seven mice infected with ChR2; n = 117 PNs from five mice infected with ArchT; light-pulse duration, 30 ms). Bins of 5 ms. Error bars, mean  $\pm$  s.e.m.



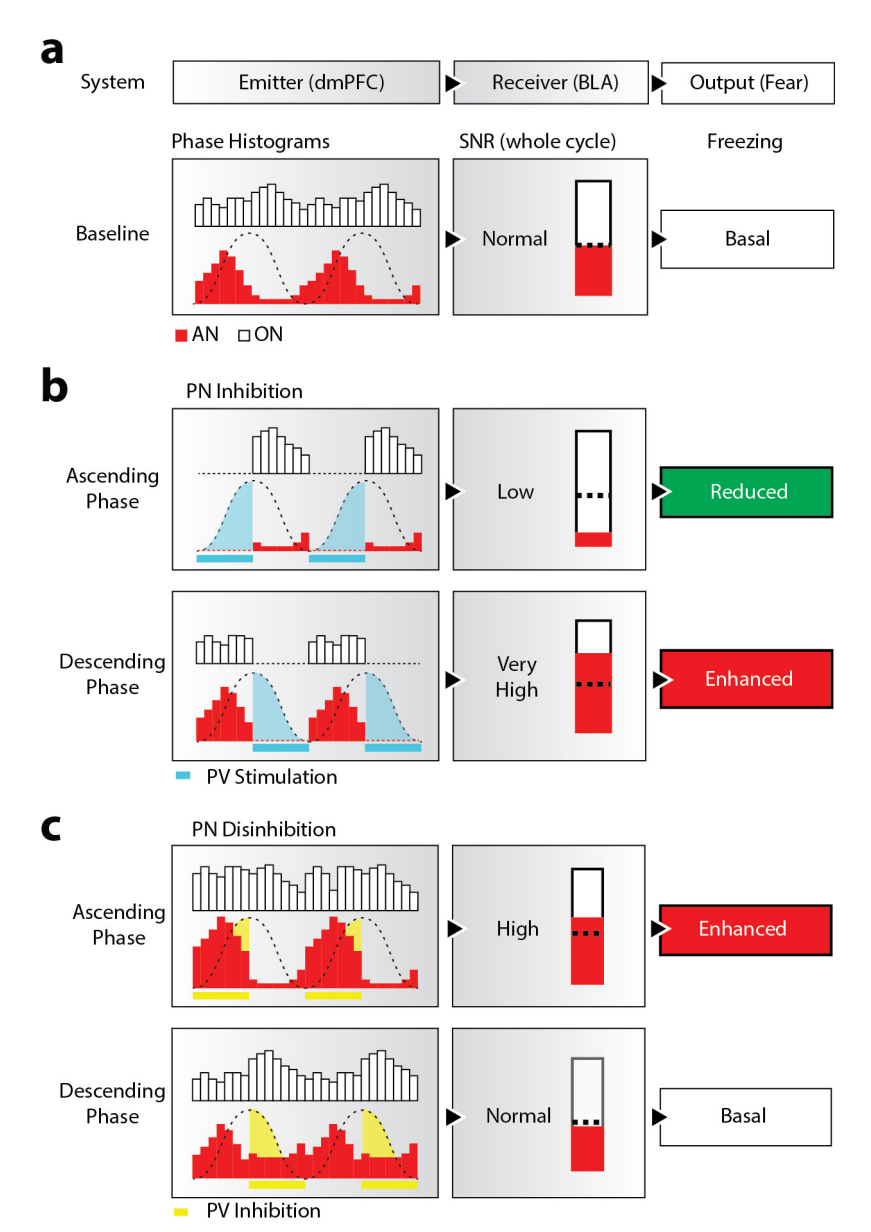
Extended Data Figure 8 | Effect of phase-specific PV manipulation on dmPFC co-firing activity. a, b, Top: corrected pairwise co-firing for pairs of dmPFC neurons recorded in mice infected with ChR2 or GFP during stimulation in the ascending (a, ChR2, n = 2,877 pairs; GFP, n = 2,067 pairs) or descending (b, ChR2, n = 2,067 pairs; GFP, n = 2,282 pairs) phase of 4 Hz oscillations. Bottom: averaged delta-corrected pairwise co-firing activity (delta = ChR2 minus GFP) as a function of 4 Hz phase (one sample t-test with Bonferroni correction, hypothetical mean = 0, \*\*P < 0.01,

\*\*\*P < 0.001). **c**, **d**, Top: corrected pairwise co-firing for pairs of dmPFC neurons recorded in mice infected with ArchT or GFP during stimulation in the ascending (**a**, ArchT, n = 2,389 pairs; GFP, n = 2,542 pairs) or descending (**b**, ArchT, n = 3,122 pairs; GFP, n = 2,282 pairs) phase of 4 Hz oscillations. Bottom: averaged delta-corrected pairwise co-firing activity (delta = ArchT minus GFP) as a function of 4 Hz phase (one-sample t-test with Bonferroni correction, hypothetical mean = 0, \*P < 0.05, \*\*P < 0.01, \*\*\*P < 0.001). Error bars, mean  $\pm$  s.e.m.



Extended Data Figure 9 | Phase-specific optogenetic disinhibition of dmPFC PNs enhanced fear behaviour. a, Timeline scheme for the optogenetic stimulation protocol on day 3 with stimulation targeting the descending phase of 4 Hz oscillation cycle (top) and day 4 with stimulation targeting the ascending phase of 4 Hz oscillation cycle (bottom). **b**, **d**, Comparison of freezing levels between CS<sup>+</sup> 1 and CS<sup>+</sup> 2–4 for epochs 10 s preceding, during and 30 s after CS<sup>+</sup> during optogenetic stimulation of PV-IRES-Cre mice infected within the dmPFC with ArchT (pre-CS<sup>+</sup>, CS<sup>+</sup> and post-CS<sup>+</sup> respectively) on day 3 (b) and day 4 (d). On day 3, descending phase stimulation after CS<sup>+</sup> 1 had no effect on freezing levels during subsequent  $CS^+$  epochs before, during or after  $CS^+$  (n = 5 ArchT mice, repeated-measures two-way ANOVA, factor 1: CS<sup>+</sup> 1 versus CS<sup>+</sup> 2–4, P > 0.05; factor 2: epoch, P < 0.05;  $F_1 \times F_2$ , P > 0.05; Student– Newman–Keuls post-hoc test within factor 1, \*\*P < 0.01 compared with both pre- and post-CS<sup>+</sup> epochs, \*P < 0.05 comparing pre-CS<sup>+</sup> with CS<sup>+</sup> epochs). On day 4, ascending phase stimulation after CS<sup>+</sup> 1 had no effect on freezing levels during subsequent CS<sup>+</sup> epochs before, during or after  $CS^+$  (n = 5 ArchT mice, repeated-measures two-way ANOVA, factor 1:

 $CS^+$  1 versus  $CS^+$  2–4, P > 0.05; factor 2: epoch, P < 0.05;  $F_1 \times F_2$ , P < 0.05; Student–Newman–Keuls post-hoc test within factor 1, \*\*\*P < 0.001 compared with both  $CS^+$  and post- $CS^+$  epochs, \*P < 0.05 comparing pre-CS<sup>+</sup> with CS<sup>+</sup> epochs). c, e, Left: time-resolved changes in freezing behaviour during light-mediated inhibition of dmPFC neuronal assemblies in the descending (c) or ascending (e) phase of the 4 Hz oscillation in PV-IRES-Cre mice infected within the dmPFC with ArchT (descending phase: first CS<sup>+</sup>, n = 5; ascending phase: first CS<sup>+</sup>, n = 5) or GFP (descending phase: first CS<sup>+</sup>, n = 7; ascending phase: first CS<sup>+</sup>, n = 4; descending phase: two-way ANOVA, factor 1: ArchT versus GFP, P > 0.05; factor 2: time, P > 0.05;  $F_1 \times F_2$ , P > 0.05; ascending phase: two-way ANOVA, factor 1: ArchT versus GFP, P < 0.01; factor 2: time, P < 0.01;  $F_1 \times F_2$ , P < 0.01). Shaded area represents the period during which the light stimulation was applied. Right: averaged freezing behaviour during the stimulation in the descending (c) (ArchT n = 5; GFP n = 7, Mann-Whitney test, ArchT versus GFP, P > 0.05) or ascending phase (e) (ArchT n = 5; GFP n = 4, Mann–Whitney test, ArchT versus GFP, \*P < 0.05). Error bars, mean  $\pm$  s.e.m.



Extended Data Figure 10 | Functional model of phase-specific coding for freezing behaviour. This schematic illustrates how, within a 4 Hz cycle, the phase specificity and relative influence of dmPFC assembly and non-assembly neurons (AN, ON, respectively) could represent a functional signal for downstream structures implicated in the expression of freezing behaviour. a, In normal freezing conditions, the prevalence and restriction of AN activation in the ascending phase combined with the monotonic phase distribution of ONs provides downstream structures with a signal-to-noise ratio (SNR) over an entire 4 Hz cycle that allows freezing expression. b, During optogenetic PN inhibition this SNR is altered. Top: when stimulating in the ascending phase, the bulk of AN activity over a cycle is shut down. This dramatically reduces SNR and prevents freezing expression. Bottom: when stimulating in the descending phase, AN

activity is largely preserved over a cycle while that of ONs is diminished to a large extent. This strongly increases SNR and exacerbates freezing expression. c, During optogenetic PN disinhibition the SNR is also altered. Top: when stimulating in the ascending phase, the AN activity over a cycle is promoted compared with non-ensemble activity. This increases SNR and enhances freezing expression. Bottom: when stimulating in the descending phase, both assembly and non-assembly neuron activities over a cycle are increased. This does not affect SNR and freezing remains similar to normal conditions. In this model the dmPFC can be seen as an emitter whose signal transmission conditions the SNR for the receiver and the further expression of fear behaviour. Our optogenetic dissection of phase specificity for dmPFC neuronal assemblies shows that SNR can be manipulated to either.